Specialized color modules in macaque extrastriate brain

Bevil R. Conway1, Sebastian Moeller2 and Doris Y. Tsao2
1Neuroscience Program, Wellesley College, 2Institute for Brain Research and Center for Advanced Imaging, University of Bremen
Address correspondence to BRC, bconway@wellesley.edu

It is unclear how the brain determines hue. Imaging studies are consistent with the existence of specialized color regions in the brain, but electrophysiological studies have produced conflicting results. Here we address the neural basis for color, using targeted single-unit recording in alert macaque monkeys, guided by functional magnetic resonance imaging (fMRI) of the same subjects. Distributed within posterior inferior temporal cortex, a large region encompassing V4, PITd and posterior TEO that some have proposed functions as a single visual complex, we found color-biased fMRI hotspots, which we call "globs", each several millimeters wide. Almost all cells located in the globs showed strong luminance-invariant color tuning, and some shape selectivity; cells in different globs represented distinct visual field locations, consistent with the coarse retinotopy of this brain region. Cells in "inter-glob" regions were not color-tuned, but more strongly shape-selective. Neither population was direction-selective. These results argue that color perception is mediated by specialized neurons that are clustered within the extrastriate brain.

In humans and macaque monkeys, color vision depends on the differential responses of three types of cones, but it is unclear how the brain ultimately uses these signals to achieve hue. ("Hue" is often used interchangeably with "color", although technically color consists of hue, saturation and brightness). On a gross level, it remains disputed whether color is localized to a particular brain region; on a microscopic level, it is uncertain what contribution single cells make to the perception of specific hues. While some brain imaging studies have suggested that color processing may be localized within the extrastriate brain (Beauchamp et al., 1999; Conway and Tsao, 2006; Hadjikhani et al., 1998; Wade et al., 2002; Zeki et al., 1991), single-cell electrophysiological studies, which have higher spatial and temporal resolution than imaging, have produced conflicting results (Kruger and Gouras, 1980; Kusunoki et al., 2006; Schein and Desimone, 1990; Schein et al., 1982; Tanaka et al., 1986; Van Essen and Zeki, 1978; Zeki, 1973), and cast doubt on the notion of a specialized color center (Gegenfurtner and Kiper, 2003; Schiller, 1996). But in addition to severe sampling limitations, single-cell studies have been frustrated because of difficulties defining color itself, and defining appropriate electrophysiological criteria. Most cells at the first cortical stage of visual processing, V1, show color biases among different colored stimuli matched in luminance (Lennie et al., 1990). The only signal distinguishing such "equiluminant" stimuli would seem to be hue. But hue biases of V1 cells are often altered or entirely abolished when the stimuli are raised or lowered in luminance (Solomon and Lennie, 2007), unlike hue perception. Thus the "color biases" of many V1 neurons may be an artifact not relevant to color vision (Solomon and Lennie, 2005), attributed instead to random cone clustering. For a neuron to contribute to color, it would seem important to show not only that it has hue selectivity to equiluminant stimuli, but also that it retains hue selectivity at different luminance levels. Within V1, 5-10% of cells show color preferences despite changes in luminance (Conway, 2001; Conway and Livingstone, 2006). These cone-opponent cells are often specialized to respond to color contrast (Conway, 2001; Conway et al., 2002; Conway and Livingstone, 2006; Horwitz et al., 2007; Johnson et al., 2004; Wachtler et al., 2003), but show hue tuning to only a restricted set of colors, close to the cardinal directions in color space (red-cyan and blue-yellow) (Conway, 2001; Conway and Livingstone, 2006).

These cells are likely building blocks for hue, but where and how the brain computes specific hues—red, orange, yellow, brown, cyan, blue, and purple—remains mysterious.

One possibility is that specialized color cells in V1 serve as building blocks for hue-specific neurons located in brain regions at subsequent stages of visual processing. One influential single-unit study proposed that V4 was the "color area", containing 100% hue-selective cells (Zeki, 1973); this claim was disputed by lesion studies (Heywood et al., 1992; Schiller, 1993; Walsh et al., 1993) and later single-unit studies (Kruger and Gouras, 1980; Schein and Desimone, 1990; Schein et al., 1982; Tanaka et al., 1986; Van Essen and Zeki, 1978), one of which reported that only 16% of V4 neurons show hue tuning. The discrepancy regarding the proportion of hue-selective cells in V4 has been attributed to differences in the shape of stimuli used(Kruger and Gouras, 1980), differences in the way neurons were classified(Schein and Desimone, 1990), and may also be attributed to differences in luminance of the stimuli used. A luminance-invariance color test has not been previously been applied, leaving open the possibility that the color tuning of V4 "color" cells, like that of most V1 cells, is an artifact of the luminance of the stimulus used. Alternatively, different studies may have come to different conclusions because of functional heterogeneity within this region. Finally, many of the studies that have contributed to this debate were conducted in anaesthetized animals. Anesthetics not only dampen cortical activity, but also can dramatically alter tuning properties (Pack et al., 2001).

Current opinion (Gegenfurtner and Kiper, 2003; Schiller, 1996) is that V4 contributes to shape perception, visual attention and perhaps stereopsis, and not exclusively or especially color (Hegde and Van Essen, 2005; Hinkle and Connor, 2002; Motter, 2006; Pasupathy and Connor, 1999; Pollen et al., 2002; Reynolds and Chelazzi, 2004). The role of V4 in color remains unresolved; recent studies have focused instead on brain regions immediately anterior to V4, including posterior TEO (Tootell et al., 2004), and PITd (Conway and Tsao, 2006), and other regions even further anterior (Komatsu et al., 1992), although the functional organization of V4, PITd and posterior TEO, and the relationship of these regions to each other, is debated (Boussaoud et al., 1991; Brewer et al., 2002;

Fize et al., 2003; Tootell et al., 2004; Zeki, 1996). Some have argued that this entire region of posterior inferior temporal cortex functions as a single visual complex (Zeki, 1996). Here we re-evaluate the role of this brain region in processing color, in the alert macaque, by combining whole-brain functional imaging with targeted single unit physiology in the same subjects. We find that color responses are clustered in hotspots each several millimeters wide, a functional organization that may account for discrepancies in conclusions regarding the role of this region in color perception.

Results

fMRI experiments

We have previously used functional magnetic resonance imaging (fMRI) to identify downstream brain regions of the alert macaque that may be involved in color, by comparing the responses to equiluminant colored gratings with responses to achromatic gratings (Conway and Tsao, 2006). Here we repeated that experiment, but using a contrast agent (ferumoxtran-10, Guerbet, Paris). Consistent with the previous report, color-biased activity was found in V1 and V2, as well as in regions of posterior inferior temporal cortex, anterior to the anterior boundary of V3. In the present study, fMRI responses were determined in four macaques (Figure 1&2; Supplementary Figures 2&3). Here we focus on the region anterior to V3, which consists of classically defined V4 and adjacent regions known variously as PITd, V4A, and posterior TEO [see (Conway and Tsao, 2006) for review].

.

Color-biased activity in this region is not uniform, but localized to discrete, reproducible hotspots. We have adopted the term “glob” to describe these hotspots. This term draws an analogy with the cytochrome-oxidase blobs of V1, which are rich in color-opponent cells (Livingstone and Hubel, 1984; Lu and Roe, 2007). The location and number of globs varies somewhat from animal to animal, although within any given animal they are reproducible (compare data sets 1 and 2 in Figure 1 and Supplementary Figure 2). Despite some inter-animal variability, most animals showed a prominent glob in the posterior bank of the superior temporal sulcus, which we have referred to by the anatomical name PITd (Conway and Tsao, 2006) see also(Zeki, 1977); this glob may be

subdivided into posterior and anterior parts (labels "2" and "3" Figure 1 left hemisphere, and Figure 2; Figure 3C&D). Animals also often had a glob located at the anterior wall of the lunate sulcus (label "1", Figure 1&2; Figure 3C,D right panels); another, at the base of the inferior occipital sulcus (label "6", Figure 1&2; Figure 3B left panel); and another, at the base of the occipital temporal sulcus (label "7", Figure 1; Figure 3A). Several animals also had a glob on the lunate gyrus (label "4", Figure 1&2; Figure 3E), and color-biased hotspots extending further anterior into inferior temporal cortex (e.g. label "5" Figure 1&2). In all animals tested, there was a lack of color-biased activity on the dorsal half of the lunate gyrus ("inter-glob" marker, Figure 3E) and weak or no color-biased activity in V3. In several animals a stripe pattern was discernable in V2 (see dorsal V2, Figure 2), consistent with the alignment of color-coding cells with the V2 cytochrome-oxidase thin stripes (Hubel and Livingstone, 1987).

Single-unit experiments: shape selectivity

FMRI provides only a coarse assay of brain function: the size of each voxel encompasses tens of thousands of cells and the neural basis for the fMRI signal is unknown. We therefore made electrophysiological recordings of the responses of single cells, in alert fixating animals, using tungsten microelectrodes, targeting the recordings to globs and inter-globs in two animals in which we had characterized the functional architecture using fMRI. Figure 3 and Supplementary Figure 4 show the globs that were targeted for single-unit recording.

Neurons were tested with a battery of stimuli to assess shape selectivity, direction selectivity and color selectivity. Stimuli consisted of bars, in which the length, width, orientation and color were systematically varied. Figure 4A,B shows orientation/direction-tuning plots and length-tuning curves for three glob cells and three inter-glob cells. Supplementary Figures 5&6 show response functions for 30 glob and 30 inter-glob cells. Figures 4C-E show population responses. Neurons in both globs and inter-globs were often tuned for stimulus orientation (Figure 4C), although as a population, inter-glob cells were significantly more orientation selective (Figure 4, legend). Cells in both compartments were rarely direction selective (Figure 4D), yet

strongly selective for stimulus length (Figure 4E); inter-glob cells were significantly more bar-length selective (Figure 4 legend). Cells in both compartments were often length-summating (Figure 4A&B; Supplementary Figures 5&6), responding optimally to the longest bar used (16°). This shows that cells in both compartments encode information about stimulus shape, but not stimulus motion, confirming previous reports of shape selectivity in this region of brain (Desimone and Schein, 1987; Desimone et al., 1985; Girard et al., 2002; Gustavsen and Gallant, 2003; Kobatake and Tanaka, 1994; Pasupathy and Connor, 1999). But the differences in orientation-tuning and length-selectivity between glob and inter-glob cells suggest that inter-glob cells perform more elaborate shape computations than glob cells.

Single-unit experiments: color selectivity

Figure 5 shows color-response measurements for a typical cell in a glob (Figure 5A), inter-glob (Figure 5B) and, as a further control, area MT (Figure 5C). These measurements were conducted by presenting an optimally configured bar at the center of the response region for each cell, and in each trial changing the color of the bar. In the post-stimulus time histograms shown in Figure 5 (left panels), the responses have been sorted according to the color of the bar. Note that the histograms are *not* raster plots: the responses to each color shown along a given row are the average of many presentations of the given color. The top two rows in each histogram show the responses to white and black. The rest of the histogram plot is divided into three sections. The top section shows responses to a set of colors that were equiluminant with each other but lower luminance than the background; the middle section shows responses to a set of colors that were equiluminant-with-background; and the bottom section shows responses to a set of colors that were equiluminant with each other but higher luminance than the background. All colors could be discriminated by human observers, even at the lowest luminance. Within each section, the responses have been arranged according to a hue cycle. The colors have been assigned a value from 0° to 352°, to reflect their position in a hue circle (Supplementary Table 1). The top row of each section shows the responses to red (0°); and the subsequent rows progress gradually through orange, yellow, green, cyan, blue, purple, ending at bluish-red (352°). Each set comprised forty-five different colors; for

ease of presentation, the responses have been compressed into 15 rows, each row showing the average response to three consecutive colors in the cycle.

Most glob cells were excited by a specific hue. The glob cell shown in Figure 5A was excited by bluish-red, shown by the maximal response density at the bottom of each section of the histogram. The hue responses can be compressed into polar coordinates (Figure 5A-C, middle panels). Polar-hue plots were generated by summing the responses following the visual latency, over the stimulus duration (200ms). Despite differences in overall response magnitude to the three color sets, the peak hue response within each color set was the same: each of the three curves in Figure 5A, middle panel, point to ~330°. This shows that the hue-selectivity was luminance invariant. Luminance-invariance can be quantified by determining the degree to which the patterns of responses to the different color sets are correlated. Luminance invariance does not imply that luminance does not sculpt the responses (it clearly modulates the magnitude of the response for many cells as in Figure 5A), just that a change in luminance does not drastically shift the hue tuning, or obliterate it by eliciting a strong response to all colors. The correlation coefficient of the response to color set 1 and color set 2 for the glob cell in Figure 5A was 0.94; between color set 1 and 3, 0.87; and between color set 2 and 3, 0.96; average, 0.92. The inter-glob cell (Figure 5B), on the other hand, did not show strong hue tuning, to any color set; what little color bias it showed, to the blue of the middle color set, was not consistent between color sets: the peak of the three curves do not point to the same direction. The MT cell (Figure 5C) similarly lacked hue tuning. Neurons like these, that do not show hue tuning to at least one of the color sets, and/or whose hue tuning is eclipsed with the introduction of luminance contrast, lack luminance-invariant hue tuning and will show weak correlation coefficients (see Figure 7B).

To further quantify the responses to this comprehensive set of colors, spanning both the hue and luminance axes of color space, we combined the responses to the three corresponding colors of each set (e.g. color 0° in the three color sets) as a weighted average, weighted by the total strength of the response to each color set (Figure 5, far right panels; similar conclusions are reached from an analysis of the responses to each

color set separately, see Supplementary Figure 7). The Rayleigh statistical test was then performed, summarizing the entire response as a vector (asterisks, Figure 5), the length of which can vary from 0, for circular distributions centered at the origin, to 1 for highly asymmetric distributions reflecting maximal hue tuning. Consistent with the hue tuning shown in the post-stimulus-time histograms, the glob cell had a significant vector (Rayleigh vector different from 0, $p<0.05$), while the inter-glob (Figure 5B) and MT (Figure 5C) cells did not.

Figure 6A shows the responses of six additional glob cells, representing a range of hue tuning, including (top to bottom) orange, green, cyan, blue, purple and red. Most glob cells (238/308; 77%) had a significant vector length. Figure 6B shows the responses of six additional inter-glob cells; all lack luminance-invariant hue tuning. Only 11% (21/192) of inter-glob cells showed significant vector lengths. MT cells also rarely showed significant Rayleigh vector lengths (1/137)

Apart from differences in receptive-field location (see Figure 8), there were no consistent differences in the response properties of cells recorded in one glob versus another, or in the globs of one animal compared to another. We therefore pooled the responses of all neurons located in globs and all those in inter-globs for a population analysis. Figure 7A shows the Rayleigh vector lengths, along the y-axis, for the population of cells. The color-to-achromatic response ratio, another measure of color sensitivity, is shown along the x-axis. The three populations are significantly different from each other, using either measure of color tuning: the vector lengths of glob cells (mean, 0.43 +/- 0.01) were longer than those of inter-glob cells (mean, 0.120 +/- 0.005; t-test significance = $8.9\text{x}10^{-96}$ with a 95% confidence interval on the mean c.i. = [0.3004 0.3472]; Kolmogorov-Smirnov (KS) test, $p<1\text{x}10^{-68}$, maximum difference in cumulative fraction, $D = 0.8$), and longer than those of MT cells (mean, 0.070 +/- 0.005; significance = $6.7\text{x}10^{-111}$, c.i. = [0.3456 0.3919]; KS test $p<1\text{x}10^{-66}$, $D= 0.88$). The vector lengths of inter-glob cells were slightly longer than those of MT cells (significance = $1.6\text{x}10^{-9}$, c.i. = [0.0307 0.0592] ; KS test $p<1\text{x}10^{-7}$, $D= 0.31$), although this distinction is not significant when

the analysis is restricted to just the equiluminant-with-background set of colors (Supplementary Figure 7 and Supplementary Table 2).

The color-to-achromatic response ratio was higher for glob cells than for inter-glob cells (significance = 6.5×10^{-34}, c.i. = [0.2567 0.3471]); KS test $p < 4 \times 10^{-28}$, $D = 0.51$) and higher than for MT cells (significance = 1.5×10^{-48}, c.i. = [0.3717 0.4668]; KS test $p < 2 \times 10^{-34}$, $D = 0.63$). The color-to-achromatic response ratio was also higher for inter-glob cells than for MT cells (significance = 9.4×10^{-7}, c.i. = [0.0712 0.1635]; KS test $p < 2 \times 10^{-5}$, $D = 0.25$). The high color-to-achromatic response ratio of glob cells (mean, 0.30 +/- 0.02) reflects the strong color tuning of this population (arrows, Figure 7A). That glob cells respond better to color than to achromatic luminance contrast is indicated in the post-stimulus-time histograms (Figures 5&6), in which the responses to black or white are rarely as strong as the strongest response to any color. The distribution of inter-glob cells (Figure 7A) is not different from zero (mean, 0.00 +/- 0.02), indicating that on average inter-glob cells responded about as well to black or white as they did to the best color; this is also indicated in Figures 5&6, in which the responses to black or white are as strong as the strongest response to any color. The mean of MT cells (-0.12 +/- 0.02), on the other hand, is skewed to negative values, showing that MT cells gave a stronger response, on average, to black or white than to the best color. The color-to-achromatic response ratio of the single-unit data is similar to that determined using the fMRI data [single-unit data of the globs, 0.30 +/- 0.02; fMRI data, 0.3 +/- 0.2 see ref (Conway and Tsao, 2006)] supporting the hypothesis that the fMRI signal is correlated with above-threshold neural activity.

Most glob cells (89%, 274/308) showed a significant correlation coefficient ($p < 0.05$) to all three pair-wise comparisons: the pattern of response to color set 1 correlated with that to color set 2; the pattern of response to color set 1 correlated with that to color set 3; and the pattern of response to color set 2 correlated with that to color set 3. This luminance-invariant hue tuning is shown by the high average correlation coefficients of the glob cells (Figure 7B). Some glob cells did, however, show weak correlation coefficients, yet high Rayleigh vector lengths (Figure 7B); these cells consist of those cells that responded

to a single color within a single color set, and no colors in any other color set. These cells are not just hue-selective but *color*-selective: "color" incorporates both hue (i.e. orange) and luminance (i.e. *dark* orange, or brown). Other glob cells showed significant correlations between all pair-wise comparisons, yet weak Rayleigh vectors. These cells usually had two peaks, on opposite sides of the hue cycle, with different time-courses (Figure 6A, fifth cell from the top). Despite their low Rayleigh vector lengths, the significance of the correlation coefficients suggests these cells are contributing to color; the multiple peaked hue tuning may represent center-surround interactions of antecedent double-opponent color cells (Conway 2001; Conway and Livingstone, 2006). Of those glob cells that did not show significant Rayleigh vector lengths, the majority (39/70) nonetheless showed significant correlations of all pair-wise comparisons. We therefore conclude that at least 90% [(238+39)/308] of glob cells showed significant hue tuning.

A minority of inter-glob cells (40%; 76/192) showed significant correlations of all pair-wise comparisons. Similarly, MT infrequently showed significant pair-wise correlations between all three color sets (20%, 27/137). As these data suggest, glob cells not only have stronger hue tuning (Figure 7A), but also stronger luminance-invariant tuning than either the inter-glob cells or MT cells (Figure 7B; KS test, $p<0.005$).

Although most inter-glob and MT cells lacked significant hue tuning, many showed some bias within one of the color sets—usually the middle set, which comprised colors that were equiluminant with the background grey. The responses to the middle set tended to be much weaker than the responses to the other two color sets, and within this weak response, the color biases were almost always for blue, but sometimes for red (Figures 5&6), reminiscent of earlier reports(Kruger and Gouras, 1980). That the bias is not present in the lowest-luminance color set suggests the bias is not attributed to selective involvement of rods. Three interpretations of these color biases are: 1, they represent genuine color preferences, usually for blue; 2, they were the result of chromatic aberration, which introduced a slight luminance artifact at the edge of the bar to which the cells were sensitive, an aberration that would be strongest for blue stimuli; and 3, they reflect a difference between macaque and human equiluminant functions, and a higher

sensitivity of macaques for blue (Dobkins et al., 2000). The color bias was usually abolished by the introduction of luminance contrast, showing that these cells do not provide a reliable representation of hue.

These results describe three separate measures of color: the Rayleigh vector length (specificity and magnitude of hue tuning), the color-to-achromatic response ratio (selectivity for hue), and the correlation coefficient (luminance-invariance of hue tuning). These provide a complete description of the color properties of single cells and each measure gives independent confirmation that glob cells are significantly more involved in color processing than either inter-glob cells or MT cells.

Discussion

This study combines two techniques to revisit the role that posterior inferior temporal cortex plays in processing color: fMRI was used to provide a coarse overview of the functional architecture, and targeted single-unit electrophysiology within the same subjects was used to provide a detailed characterization of cellular function. These two techniques provide independent confirmation of specialized modules, or globs, which contain a high fraction of luminance-invariant color-tuned neurons. These modules are separated by regions that are not specialized for color, but seem specialized for more detailed form analysis. This result reconciles the conflicting conclusions regarding color processing in and anterior to V4: reports asserting that V4 is specialized for color (Kusunoki et al., 2006; Zeki, 1973) probably targeted globs, while reports denying that V4 is specialized for color (Kruger and Gouras, 1980; Schein et al., 1982; Tanaka et al., 1986; Van Essen and Zeki, 1978) likely recorded from inter-globs. Indeed most single-unit V4 studies have not focused on color selectivity, but rather on shape processing and attentional effects (Hinkle and Connor, 2002; Pasupathy and Connor, 1999; Reynolds and Chelazzi, 2004; Schiller, 1996); these studies relied on recordings in the crest of the prelunate gyrus, the part of V4 that is most accessible but one that usually consists of an inter-glob. Inter-glob cells lacked strong color tuning but did show weak color sensitivity not present in area MT (a motion area). This sensitivity may be sufficient basis for color-based attention to modulate V4 responses (Mirabella et al., 2007; Motter, 2006): attention

may effectively increase color contrast in the same way it increases luminance contrast (Reynolds and Chelazzi, 2004). The strong color-tuning of glob cells, on the other hand, may contribute directly to hue perception and color constancy (Kusunoki et al., 2006). In addition, the finding that globs are found in several parts of inferior temporal cortex accounts for the observation that lesions of extrastriate cortex leave color vision largely intact unless the lesions are large (Cowey et al., 2001; Heywood et al., 1995; Schiller, 1993).

The present study focused on a few globs and the intervening cortex located within posterior inferior temporal cortex. Only one set of colors, at a single orientation, were used to identify the globs (because fMRI requires averaging data from many trials). The single-cell recordings in the globs showed that most of the neurons were strongly hue selective and often orientation selective, suggesting that only a subset of glob cells are responsible for the fMRI signal. That a subset of cells is sufficient to drive the fMRI response seems likely given that small changes in mean firing rate correspond to relatively large changes in fMRI signal (Heeger et al, 2000).

The receptive-field centers of cells within any one of the globs did not completely tile the visual hemi-field (Figure 8), although individual receptive-fields often covered a region over 15° wide (Figure 4A; Supplementary Figures 5&6). Judging by the location of the center of glob-cell receptive fields and by the location of globs relative to fMRI eccentricity maps (Figure 2), different globs represent different regions of the visual field, suggesting that a single glob does not constitute an entire visual area, but rather one module in a specialized network, much like the cytochrome-oxidase stripes in V2. But whether this region contains multiple representations of color, how color and shape interact, and the role of glob and inter-glob cells in processing color context will require more study.

Physiological investigations often rely on anatomical landmarks to interpret function. The assumption that function is yoked to anatomical location is justified on a coarse scale: V1 in all macaques is located at the pole of the occipital cortex. But functional imaging

shows that normal animals of the same species can show variability not only in the anatomy of their brains, but also in the relative anatomical location of functional patterns of activity and boundaries of visual areas (compare Figures 1 and 2). The variability in anatomical location becomes more marked at higher stages of visual processing, where the size of functionally defined regions can be relatively small. The middle face patch, for example, varies in its location relative to sulcal patterns and stereotaxic coordinates by several millimeters from one animal to the next, on the same scale as the size of patch itself (Tsao et al., 2003; Tsao et al., 2006). The sampling limitations of single-unit recording are exacerbated by the fact that the functional organization of more anterior brain regions is poorly understood. Brain regions V4, PITd and posterior TEO encompass a large swath of cortex for which there is no consensus of the boundaries (Brewer et al., 2002; Conway and Tsao, 2006; Fize et al., 2003; Stepniewska et al., 2005; Tootell et al., 2004); some argue the entire region is a single visual complex (Zeki, 1996). Leaving boundary disputes aside, it is clear from connectional studies that this region receives patchy inputs from other areas (Distler et al., 1993; Felleman et al., 1997; Shipp and Zeki, 1995; Xiao et al., 1999), has patchy local connections (Yoshioka et al., 1992), and patchy callosal connections (Zeki, 1977), suggesting a more complex functional organization than three discrete areas. The data here suggest that this region contains relatively large specialized color domains. We hypothesize that these domains receive input from V2 thin stripes, an hypothesis supported by the fact that the size of the globs is consistent with the size of V4 patches that receive input from V2 thin stripes (Felleman et al., 1997; Shipp and Zeki, 1995; Xiao et al., 1999). Color would then appear to be processed by a series of specialized color domains that get progressively larger at subsequent hierarchical stages: the blobs in V1, the thin stripes in V2, and the globs in posterior inferior temporal cortex; the inter-globs, on the other hand, would seem to be involved in elaborating the form signals relayed by the V1 inter-blobs and V2 inter-stripes.

It is perhaps no surprise that previous studies based on single-unit recordings guided by anatomical landmarks, yet suffering from sampling limitations imposed by single-unit recording, could come to radically different conclusions about function: large swaths of extrastriate cortex are probably not homogenous brain regions, and may consist of functional columns larger than the sampling size of single-unit recordings but smaller

than the scale of the visual area under investigation. This underscores the importance of combining functional, as opposed to solely anatomical landmarks, with single-unit recording in studying extrastriate brain.

Acknowledgments. Funded by the Alexander von Humboldt foundation (BRC, DYT) and by the German Ministry for Science and Education, Grant 01GO0506 (Bremen Center for Advanced Imaging). BRC received additional support from the Harvard Society of Fellows and the Neuroscience Program, Wellesley College. We thank Katrin Thoss, Ramatsani Hakizimana and Nicole Schweers for expert animal care; Karoline Spang and Katrin Sebald assisted calibrating monitors. David Freeman designed the physiology software; Winrich Freiwald, Heiko Stemman, Aurel Wannig, David Hubel, Margaret Livingstone and Alexander Rehding contributed to useful discussions; Guerbet provided the contrast agent. This paper is dedicated to the memory of our dear friend David C. Freeman.

Figure Legends

Figure 1 FMRI of alert fixating macaque reveals hot-spots, or "globs", of color-preferring brain activity in posterior inferior temporal cortex, the brain region anterior to V3, consisting of V4, PITd, and posterior TEO. Visual area boundaries were determined using responses to checkerboard stimuli restricted to wedges along the vertical and horizontal meridians (Supplementary Figure 1). **Top**, a computationally flattened map, the average of all data for this monkey; sulci are indicated by dark grey. **Middle,** coronal sections showing responses from two independent data sets (40 stimulus runs each; approximate anterior-posterior position indicated at right). Color-preferring regions were identified as those that responded more strongly to equiluminant colored stripes than to achromatic stripes. Labels 1-7 identify prominent globs, and facilitate a comparison between the raw slice data and the computationally manipulated flattened data. Significance depicted by color bar. LGN, lateral geniculate nucleus; s.t.s., superior-temporal sulcus; o.t.s., occipital-temporal sulcus; i.o.s., inferior-occipital sulcus; l.s., lunate sulcus.

Bottom, traces show the time course of the fMRI response to achromatic stripes (grey columns); red/blue colored stripes of various red-to-blue luminance ratios (pink columns); and responses to uniform grey (white columns). Area MT shows stronger responses to achromatic stripes than to any colored stripes, and shows a minimum to colored stripes that are approximately equiluminant (color ratios 0 and 0.33). The globs show stronger responses to all colored stripes; and the inter-globs show similar magnitude responses to color and achromatic stripes. Responses were measured using a contrast agent, which results in a negative fMRI signal (traces have been flipped vertically, and de-trended). Scale bar = 1cm.

Figure 2 FMRI of color-preferring brain activity for a second macaque. See Figure 1 for conventions. fMRI responses to the central 3° enclosed by the green contour. Globs are located both inside and outside the central 3°. Eccentricity maps were determined by measuring responses to gratings (0.29cycles/°) restricted to either the central 3° or the periphery (extending 28°, central 3° gray). These were interleaved with blank periods of

neutral gray. Gratings were achromatic in half the blocks and equiluminant in half the blocks, and data from both were averaged.

Figure 3 Magnetic resonance images showing the location of five (**A-E**) tungsten micro-electrode recordings, targeting color-preferring (glob) and non-color preferring (inter-glob) regions of alert macaque brain. Electrodes are black, highlighted by vertical white extension lines. Functional activity (response to equiluminant color > response to achromatic) is superimposed. The brain has been computationally sliced in the plane of the electrode: pseudo-frontal sections (left); pseudo-sagittal sections (right). Numbers relate to the globs identified in Figure 1; approximate A-P coordinates given in Figure 1. Supplementary Figure 4 shows electrodes targeting globs and inter-globs in a second animal. l.g., lunate gyrus; M, medial; D, dorsal; A, anterior; other conventions as for Figure 1. Scale bar is 1 cm.

Figure 4 Glob and inter-glob cells show shape selectivity and lack direction selectivity; inter-glob cells are more strongly shape selective than glob cells. **A**, length-tuning curves and orientation/direction plots (insets) for three glob cells. **B**, length-tuning curves and orientation/direction plots (insets) for three inter-glob cells; Supplementary Figures 5&6 show more examples of both. **C**, quantification of orientation selectivity; **D**, direction selectivity; and **E,** bar-length selectivity (0, no selectivity; 1, maximal selectivity). Significant indices (>0.2) are shown in dark grey. Recording positions were confirmed using MRI (Figure 3). Polar plots were generated using bars of optimal length and color, drifted through the receptive field; plots are smoothed with a moving average (3 orientations wide) and normalized to the firing rate elicited by the optimally oriented bar. Direction tuning is indicated in the polar-plot insets by comparing the magnitude of each lobe of the response. Responses to twenty stimuli (10 bar orientations; both directions of motion) were measured. Length-tuning plots were generated using drifting bars of optimal orientation and color, and various lengths. Inter-glob cells were more orientation selective than glob cells (Kolmogorov-Smirnov test, $p<10^{-21}$, maximum difference in cumulative fraction, $D = 0.41$), and had higher length-selectivity indices (KS test, $p<10^{-5}$,

D = 0.32).Background firing rate indicated by the open symbol in A&B. Standard errors shown.

Figure 5 Color-tuning of a typical glob cell (**A**), an inter-glob cell (**B**) and an MT cell (**C**). **Left panels**, post-stimulus time histograms to an optimally shaped bar of various colors. Responses were determined to white and black (top two rows in each histogram*)* and to three sets of 45 colored versions of the bar, one set darker (top section of each histogram), another equiluminant-with-the-background (middle section) and a third set, brighter (bottom section) than the neutral grey background. The colors within each set were assigned a number from 0 to 352 and were equiluminant with each other (numbers are only shown for the bright set of colors). The spectra given to the left of each histogram are schematic (Supplementary Table 1 and Supplementary Figure 8 give the C.I.E. coordinates of the stimuli). For ease of presentation, the responses to each color set have been compressed into 15 rows, each row showing the average response to three consecutive colors in the cycle. Stimulus onset aligned with 0 ms; stimulus duration (step at bottom): 200ms ON/200ms OFF; histogram bins, 1ms. Grey scale bar is average number of spikes per stimulus repeat per bin; the lack of activity immediately following stimulus onset, until about 70-90ms, indicates the response latency—the amount of time required for the signal to be pre-processed by the eyes, lateral geniculate nucleus, V1 etc. **Middle panels,** show the color-tuning to each of the stimulus sets in polar coordinates. Responses were averaged over 200ms, beginning after the visual latency of the cell. Units are spikes/stimulus repeat.
Right panels, weighted-average color response; peak normalized to the maximum response to any color. Asterisk indicates the Rayleigh vector, a standard statistical measure of the asymmetry (i.e. hue tuning) of the polar plot. The polar plots were smoothed with a moving average spanning five colors.

Figure 6 Single-cells located in globs, but not inter-globs, show strong hue tuning. **A**, responses of six glob cells: orientation-tuning curve and an icon for the optimal color/orientation (**left**), post-stimulus time histograms of the responses to a comprehensive set of colors (**middle**), and each cell's weighted-average hue-tuning, as a

polar plot within a hue circle (**right**). Orientation-tuning curve units: spikes/bar sweep. Standard Errors shown. See Figure 5 for other conventions. **B,** histograms and polar plots for six inter-glob cells. Asterisks in the polar plots indicate the Rayleigh vector.

Figure 7 Quantification of the color tuning of the population of glob cells, inter-glob cells and MT cells. **A,** The y-axis is a measure of hue tuning (the Rayleigh vector length; 0 is no tuning, 1 is maximal tuning), determined from the weighted-average responses (see Figure 5); the x-axis shows the color-to-achromatic response ratio, a measure of color selectivity, determined as $(R_{color} - R_{achromatic})/(R_{color} + R_{achromatic})$, where R_{color} is the maximum response to any color and $R_{achromatic}$ is the stronger of the black or white response. The axes of the marginal distributions are number of cells per bin. Arrows indicate population means. **B,** The y-axis shows the Rayleigh vector length; the x-axis shows the average correlation coefficient (r^2) of the hue tuning, between the three color sets, for each cell; this evaluates luminance-invariance of the color tuning (negative and 0 r^2 indicate no luminance-invariant hue tuning; 1, maximal luminance-invariance).

Figure 8 Visual-field location of the center of the receptive-fields of the single-units recorded within the different glob regions (numbers refer to globs in Figures 1, 2&3).

Supplementary Figure 1 Determination of area boundaries. Macaques viewed a checkerboard stimulus restricted to a wedge 20° wide, along the horizontal and vertical meridians (Brewer et al., 2002; Fize et al., 2003). Responses to stimulation of the horizontal meridian were subtracted from responses to stimulation of the vertical meridian to reveal the boundaries between area borders; responses were projected on a flattened map in which the cortex was computationally inflated and unpeeled with an relieving cut along the horizontal meridian that separates upper and lower V1 (dotted line, vertical meridian; solid lines, horizontal meridian; asterisk, fovea). Shown is the data for the macaque whose color responses are shown in Figure 1. Right hemisphere is shown at right; left hemisphere, at left.

Supplementary Figure 2 FMRI of color-preferring brain activity in a third macaque monkey. See Figure 1 and Figure 2 for other conventions. Coronal sections show the average of all data obtained (leftmost column), and that from two independent recording sessions. Approximate anterior-posterior position indicated to the left of each coronal section.

Supplementary Figure 3 Functional magnetic resonance imaging of color-preferring brain activity in a fourth macaque monkey. See Figure 1 for other conventions. See also Supplementary Figure 4. Approximate anterior-posterior position indicated to the left of each coronal section. Traces show the fMRI response time-course. The white region outside the brain, seen in the coronal sections, was produced by saline in the recording chamber.

Supplementary Figure 4 Magnetic resonance images showing the location of two tungsten micro-electrode recordings, targeting color-preferring (glob) and non-color preferring regions (inter-glob) of a second macaque. The functional-activity flat map for this animal is shown in Supplementary Figure 3.

Supplementary Figure 5 Orientation/direction tuning (polar plots) and bar-length tuning for thirty glob cells recorded in alert macaque. Neurons are arranged in columns: length-summating cells, top left; end-stopped cells, bottom right. Standard errors shown. Figure 4 gives other conventions and quantification.

Supplementary Figure 6 Orientation/direction tuning (polar plots) and bar-length tuning for thirty inter-glob cells recorded in alert macaque. See Supplementary Figure 5 for other conventions. Figure 4 gives quantification.

Supplementary Figure 7 Color selectivity of glob, inter-glob and MT cells, to sets of colors of lower, equal and higher luminance than the background. The weighted-average responses are shown at the bottom (see Figure 7A). Arrows indicate population averages.

In all cases, glob cells show higher average color tuning than inter-glob and MT cells (Supplementary Table 2 gives statistics).

Supplementary Figure 8 C.I.E. coordinates of the colored stimuli used in the single-unit physiology experiments (**left**); luminance of each of the stimuli and the background (**right**). See Supplementary Table 1.

Supplementary Table 1 C.I.E. values for stimuli and background used in the single-unit physiology experiments.

Supplementary Table 2 Statistical comparisons of the color tuning of glob, inter-glob and MT cells, to color sets lower, equal and higher luminance than the background. See Supplementary Figure 7.

Experimental Procedures

All animal procedures complied with the NIH Guide for Care and Use of Laboratory Animals, regulations for the welfare of experimental animals issued by the Federal Government of Germany, and stipulations of Bremen authorities.

Functional Magnetic Resonance Imaging Experiments

Four macaque monkeys were trained for a juice reward to fixate a visual display while the animals were situated in a specially designed chair fit for a horizontal bore 3T Siemens scanner. Red&blue and achromatic gratings were presented in separate blocks interleaved with blocks of uniform grey, maintaining a constant mean luminance of 19.3 cd/m^2; maintaining a constant mean luminance ensures the cone excitation ratios are equalized across stimuli. The gratings were low spatial frequency gratings (0.29 cycles/°), drifting at 0.29cycles/°, alternating direction every 2 seconds, and had a trapezoidal-shaped waveform, incorporating the advantages of a square wave (which gives optimal contrast at each stimulated location) and a sine wave (which minimizes chromatic aberration at the 'edges' of each grating cycle (Tootell et al, 2004). We used the colors red and blue because they should activate both groups of cardinal color cells (red-cyan and blue yellow) in early visual cortex (Conway and Livingstone, 2006). Using red and blue also enables a direct comparison with other studies, using similar methods (Conway and Tsao, 2006; Tootell et al., 2004). In an initial set of BOLD scans, we used 9 colored blocks, separated by blocks of grey. The luminance ratios of the colors in each block were -0.75, -0.5, -0.33, -0.17, 0, 0.17, 0.33, 0.5 or 0.75, where contrast is [R-B]/[R+B], and R and B are the photometric luminance of the red and blue (measured using the Minolta Chromometer CS-100). We used the minimal response of MT to determine which color contrast was functionally equiluminant (Conway and Tsao, 2006; Dobkins et al., 2000). The equiluminant stimulus (luminance ratio 0.33) was determined to have L-cone-contrast 0.33, M-cone-contrast 0.38 and S-cone-contrast 0.98, where L-cone-contrast = $|(L_{red}-L_{blue})/(L_{red}+L_{blue})|$, L_{red} is the L activity elicited by the red phase of the stimulus and L_{blue} is the L activity elicited by the blue phase (Stockman and Sharpe, 2000). In subsequent experiments we injected into the femoral vein prior to each scan session a contrast agent, ferumoxtran-10 (Sinerem, Guerbet, France; Combidex,

Advanced Magnetics Inc, USA; concentration: 21 mg Fe/ml in saline; dosage: 8 mg Fe/kg). Sinerem is the same contrast agent as MION, produced under a different name (Nelissen et al., 2006); Sinerem/MION increases signal-to-noise and gives finer spatial localization than BOLD (Leite et al., 2002; Vanduffel et al., 2001; Zhao et al, 2006), although it may "not necessarily represent equivalent transforms [as BOLD] of the neural response" (Smirnakis et al, 2007). For these experiments the color-luminance ratios were -0.5, 0, 0.33, and 0.75, and block length was 32 seconds. Area boundaries were determined by the responses to vertical and horizontal meridians (Supplementary Figure 1). Voxel size was 1.25 mm^3 for most experiments; and 1.5mm^3 in a few, yielding qualitatively similar results. Data from all globs (color bias $p<0.05$) located in area V4 and the immediately adjacent anterior area were pooled to generate time courses shown; time courses from individual globs were consistent (data not shown). Glob number and location were consistent for color-to-achromatic comparisons at all color ratios, indicating that a precise determination of equiluminance was not critical for identifying globs (globs consistently showed higher activity than interglobs to all color ratios; see time-courses in Figures 1&2). Fixation was continuously monitored during all experiments using an ISCAN infra-red eye monitor (ISCAN, Burlington, MA), and monkeys were only rewarded for maintaining constant fixation. Data analysis was performed using FREESURFER software (http://surfer.nmr.mgh.harvard.edu/). Data were motion-corrected with AFNI motion correction algorithm (Cox and Hyde, 1997), and intensity normalized. Spatial smoothing was not applied to the raw functional data (as shown in the slices), but was applied to the flat maps (fwhm = 1.5 mm). More detailed methods are given elsewhere (Conway and Tsao, 2006; Tsao et al., 2006; Tsao et al., 2003).

Single unit recording

Detailed methods for single-unit recording in alert macaques are given elsewhere(Conway, 2001; Conway and Livingstone, 2006; Tsao et al., 2006). In the present experiments, a plastic MRI-compatible recording chamber (1.5cm wide; Crist Instruments, MD) was first implanted over the region of interest using standard surgical procedures. A plastic cylinder containing a matrix of holes (15 evenly spaced holes each

0.7mm wide spanned the diameter) was fitted to the inside of the recording chamber and could be locked in place using a set screw. The holes were filled with viscous silicone, which provided sufficient contrast so that individual holes could be seen in high-resolution anatomical magnetic resonance (MR) images. Previously acquired functional images were then aligned to the high-resolution images and computationally re-sliced in coordinates defined by the cylinder matrix. Tungsten micro-electrodes, sheathed in plastic guide tubes, could then be inserted through the holes of the grid matrix and lowered into the brain to target specific functional domains, as confirmed by MRIs with electrodes in place (see below). Recordings were made through a total of 34 holes in one animal and 11 holes in a second animal; multiple penetrations were made through many holes, especially those that targeted the globs in the superior temporal sulcus, on the lunate gyrus, and in the occipital temporal suclus (a total of 5 globs were targeted, indicated in Figure 3 and Supplementary Figure 4). From these penetrations, we obtained orientation-tuning curves for 365 visually responsive glob cells and 232 inter-glob cells; bar-length-tuning curves, for 85 glob cells and 104 inter-glob cells; and complete color tuning responses, for 308 glob cells and 192 inter-glob cells. Two additional penetrations were made into the glob at the base of the inferior occipital sulcus of the animal shown in Figure 2 (2 cells), and one that was presumed to be on the anterior wall of the lunate sulcus (2 cells) of a third animal, although a confirmation MRI was not made (see below). These four cells were all significantly color tuned, showing significant Rayleigh vector lengths and stronger responses to color vs. black & white (as described in the Results Section). As an additional control, recordings were made in area MT, which was traversed in penetrations targeting the ventral surface of the brain in one animal (Figure 3A&B; 52 cells); MT recordings were also made in another animal previously fitted with a dedicated MT-targeting chamber (85 cells). Data from these two animals were pooled as the responses between animals were not significantly different along any of the dimensions tested.

Single-unit responses were measured in alert fixating animals using routine electrophysiological recording procedures(Conway, 2001; Conway and Livingstone, 2006; Tsao et al., 2006) and apparatus (BAK electronics, MD). These experiments were done outside the MR scanner but with the animal seated in the same chair as used in the

fMRI experiments. Precise measurements of electrode depth were kept, documenting the initial entrance of the electrode into the brain, the depth of any white-grey matter junctions, and any exits and re-entrances of the electrode if it passed through a sulcus. Following most recording sessions, with the electrode still in position at the end of the penetration, the electrode was carefully glued to the plastic guide tube and the electrode advancer removed. The animal was transferred to the MR scanner and a high-resolution anatomical scan was made to confirm the location of the electrode (Figure 3; Supplementary Figure 4). By combining the information from the anatomical scans and the depth information obtained during the recordings, the locations of the recorded cells were correlated with the functional maps and categorized as residing in a glob or an inter-glob. Recordings were specifically targeted to avoid the edges of the globs to circumvent ambiguity about this categorization. With the exception of one penetration, all visually responsive cells from a given penetration were assigned to either a glob or an inter-glob (or area MT). The exception is shown in Figure 3E, in which the first part (3.5mm) of this long penetration was in an inter-glob; the next 0.75mm, a transition zone, was excluded from analysis; and the last part (1mm) was in a glob (the very tip of the electrode is not visible in the MRI).

Visual stimuli for single-unit experiments: shape & direction

Stimuli for the single-unit experiments consisted of an oriented bar or square patch presented on a color-calibrated computer monitor (NEC Display Solutions, Munich) that displayed uniform neutral grey surrounding the stimulus, and between stimulus presentations (CIE x, y, luminance: 0.316, 0.314, 3.05 cd/m^2, maintaining chromatically neutral photopic adapting conditions; monitor 57cm from the eyes). These stimuli elicited reliable, strong responses (see Supplementary Figures 5&6). Preliminary hand mapping was first done to determine the location of the center of the receptive field, along with the optimal dimensions of the stimulus (bar orientation, length, width and color). Shape selectivity (Figure 4, Supplementary Figures 5&6) was then quantified, using a bar of optimal color, as follows: the orientation index was $(O_{best}-O_{orthogonal})/ (O_{best}+O_{orthogonal})$, where O_{best} was the response to bars whose orientation elicited the strongest response, and $O_{orthogonal}$ was the response to bars oriented orthogonal to the best orientation. The

direction index was $(D_{pref}-D_{null})/ (D_{pref}+D_{null})$, where D_{pref} was the response elicited by the optimally oriented bar moving in the direction that elicited the strongest response, and D_{null} was the response elicited by the optimally oriented bar moving in the opposite direction (the bars in the orientation/direction experiments were optimal length). The length-selectivity index was $(L_{max}-L_{min})/ (L_{max}+L_{min})$, where L_{max} was the response to the bar length that elicited the strongest response and L_{min} was the response to the bar length that elicited the smallest response (both bars were the same, optimal, orientation). Significant responses were defined as those showing an index >0.2 (maximum response > 1.5X minimum response). Bar lengths were 0.13°, 0.25°, 0.5°, 1°, 2°, 4°, 8° and 16°.

Visual stimuli for single-unit experiments: hue

To quantify the hue selectivity, optimal stimulus dimensions (bar length, width and position) were used for each cell. The shape and location was fixed for a given cell, and the color of the shape was then varied. A total of 135 colors were used, consisting of 3 sets of 45 colors; the colors within a set were equiluminant with each other, spanned the full color gamut of the monitor, and were as saturated as the monitor could produce (CIE coordinates given in Supplementary Table 1 and Supplementary Figure 8). The colors of one set were brighter (7.8 cd/m^2) than the background; those of another set were photometrically equiluminant with the background (3.05 cd/m^2); and those of the third set were darker than the background (0.62 cd/m^2). All colors, including those at the lowest luminance, had discernable color to human observers, indicating significant activation of cones. The two color sets of equal or higher luminance than the adapting background were vividly colored, photopic, and likely did not involve rods; stimuli of the lowest luminance set may be considered mesopic and have involved rods, but this is unlikely because they were surrounded by an adapting background that maintained photopic conditions. In any event, significant hue tuning was found to stimuli of all luminance levels, showing all stimuli involve mechanisms dependent on cones (see Figures 5 & 6). Responses to black (0.02 cd/m^2) and white (78.2 cd/m^2) were also measured. These were the maximal achromatic contrast that could be achieved, which were used because they provide the maximal stringency for categorizing a neuron as color coding, according to the color-to-achromatic response ratio (Figure 7A). The different colors were presented in

pseudo-random order. Within the time period during which the three sets of colors were presented, white and black versions of the stimulus were each presented three times, so that one complete cycle consisted of 144 stimulus presentations (color set 1, 45 colors; color set 2, 45 colors; color set 3, 45 colors; white, 3X; black, 3X). Responses of a given cell were measured to multiple presentations of this cycle and averaged. Each stimulus was displayed for 200 ms, and separated in time from the previous and subsequent stimuli by 200 ms, during which time the animal was rewarded for maintaining constant fixation. Every visually responsive cell was tested and included in the analysis if responses to at least two complete stimulus cycles were obtained; in most cases the cell was held long enough so that we could measure the responses to at least 5 stimulus cycles. To generate the hue-tuning polar plots (Figures 5&6), responses were summed during a 200 ms window, a duration defined by the duration of the stimulus. The time window began with the visual latency, which was defined as >3 standard deviations above the background firing rate. The major conclusions of the paper were not affected if shorter (50ms) or longer (250ms) time windows were used.

References

Beauchamp, M. S., Haxby, J. V., Jennings, J. E., and DeYoe, E. A. (1999). An fMRI version of the Farnsworth-Munsell 100-Hue test reveals multiple color-selective areas in human ventral occipitotemporal cortex. Cereb. Cortex *9*, 257-263.

Boussaoud, D., Desimone, R., and Ungerleider, L. G. (1991). Visual topography of area TEO in the macaque. J. Comp. Neurol. *306*, 554-575.

Brewer, A. A., Press, W. A., Logothetis, N. K., and Wandell, B. A. (2002). Visual areas in macaque cortex measured using functional magnetic resonance imaging. J. Neurosci. *22*, 10416-10426.

Conway, B. R. (2001). Spatial structure of cone inputs to color cells in alert macaque primary visual cortex (V-1). J. Neurosci. *21*, 2768-2783.

Conway, B. R., Hubel, D. H., and Livingstone, M. S. (2002). Color contrast in macaque V1. Cereb Cortex *12*, 915-925.

Conway, B. R., and Livingstone, M. S. (2006). Spatial and temporal properties of cone signals in alert macaque primary visual cortex. J. Neurosci. *26*, 10826-10846.

Conway, B. R., and Tsao, D. Y. (2006). Color architecture in alert macaque cortex revealed by FMRI. Cereb. Cortex *16*, 1604-1613.

Cowey, A., Heywood, C. A., and Irving-Bell, L. (2001). The regional cortical basis of achromatopsia: a study on macaque monkeys and an achromatopsic patient. European J. Neurosci. *14*, 1555-1566.

Cox, R. W., and Hyde, J. S. (1997). Software tools for analysis and visualization of FMRI data. NMR in Biomedicine *10*, 171-178.

Desimone, R., and Schein, S. J. (1987). Visual properties of neurons in area V4 of the macaque: sensitivity to stimulus form. J. Neurophysiol. *57*, 835-868.

Desimone, R., Schein, S. J., Moran, J., and Ungerleider, L. G. (1985). Contour, color and shape analysis beyond the striate cortex. Vision Res. *25*, 441-452.

Distler, C., Boussaoud, D., Desimone, R., and Ungerleider, L. G. (1993). Cortical connections of inferior temporal area TEO in macaque monkeys. J. Comp. Neurol. *334*, 125-150.

Dobkins, K. R., Thiele, A., and Albright, T. D. (2000). Comparison of red-green equiluminance points in humans and macaques: evidence for different L:M cone ratios between species. J. Opt. Soc. Am., A *17*, 545-556.

Felleman, D. J., Xiao, Y., and McClendon, E. (1997). Modular organization of occipito-temporal pathways: cortical connections between visual area 4 and visual area 2 and posterior inferotemporal ventral area in macaque monkeys. J. Neurosci. *17*, 3185-3200.

Fize, D., Vanduffel, W., Nelissen, K., Denys, K., Chef d'Hotel, C., Faugeras, O., and Orban, G. A. (2003). The retinotopic organization of primate dorsal V4 and surrounding areas: A functional magnetic resonance imaging study in awake monkeys. J. Neurosci. *23*, 7395-7406.

Gegenfurtner, K. R., and Kiper, D. C. (2003). Color vision. Annu. Rev. Neurosci. *26*, 181-206.

Girard, P., Lomber, S. G., and Bullier, J. (2002). Shape discrimination deficits during reversible deactivation of area V4 in the macaque monkey. Cereb. Cortex *12*, 1146-1156.

Gustavsen, K., and Gallant, J. L. (2003). Shape perception: complex contour representation in visual area V4. Curr. Biol. *13*, R234-235.

Hadjikhani, N., Liu, A. K., Dale, A. M., Cavanagh, P., and Tootell, R. B. (1998). Retinotopy and color sensitivity in human visual cortical area V8. Nat. Neurosci. *1*, 235-241.

Heeger, D.J., Huk, A.C., Geisler, W.S., Albrecht, D.G. (2000). Spikes versus BOLD: what does neuroimaging tell us about neuronal activity? Nat. Neurosci. *3*, 631-3.

Hegde, J., and Van Essen, D. C. (2005). Stimulus dependence of disparity coding in primate visual area V4. J. Neurophysiol. *93*, 620-626.

Heywood, C. A., Gadotti, A., and Cowey, A. (1992). Cortical area V4 and its role in the perception of color. J. Neurosci. *12*, 4056-4065.

Heywood, C. A., Gaffan, D., and Cowey, A. (1995). Cerebral achromatopsia in monkeys. Euro. J. Neurosci. *7*, 1064-1073.

Hinkle, D. A., and Connor, C. E. (2002). Three-dimensional orientation tuning in macaque area V4. Nat. Neurosci. *5*, 665-670.

Horwitz, G. D., Chichilnisky, E. J., and Albright, T. D. (2007). Cone inputs to simple and complex cells in V1 of awake macaque. J. Neurophysiol.. *97*, 3070-81.

Hubel, D. H., and Livingstone, M. S. (1987). Segregation of form, color, and stereopsis in primate area 18. J. Neurosci. *7*, 3378-3415.

Johnson, E. N., Hawken, M. J., and Shapley, R. (2004). Cone inputs in macaque primary visual cortex. J. Neurophysiol. *91*, 2501-2514.

Kobatake, E., and Tanaka, K. (1994). Neuronal selectivities to complex object features in the ventral visual pathway of the macaque cerebral cortex. J. Neurophysiol. *71*, 856-867.

Komatsu, H., Ideura, Y., Kaji, S., and Yamane, S. (1992). Color selectivity of neurons in the inferior temporal cortex of the awake macaque monkey. J. Neurosci. *12*, 408-424.

Kruger, J., and Gouras, P. (1980). Spectral selectivity of cells and its dependence on slit length in monkey visual cortex. J. Neurophysiol. *43*, 1055-1069.

Kusunoki, M., Moutoussis, K., and Zeki, S. (2006). Effect of background colors on the tuning of color-selective cells in monkey area V4. J. Neurophysiol. *95*, 3047-3059.

Leite, F. P., Tsao, D., Vanduffel, W., Fize, D., Sasaki, Y., Wald, L. L., Dale, A. M., Kwong, K. K., Orban, G. A., Rosen, B. R.*, et al.* (2002). Repeated fMRI using iron oxide contrast agent in awake, behaving macaques at 3 Tesla. Neuroimage *16*, 283-294.

Lennie, P., Krauskopf, J., and Sclar, G. (1990). Chromatic mechanisms in striate cortex of macaque. J. Neurosci. *10*, 649-669.

Livingstone, M. S., and Hubel, D. H. (1984). Anatomy and physiology of a color system in the primate visual cortex. J. Neurosci. *4*, 309-356.

Lu, H. D., and Roe, A. W. (2007). Functional organization of color domains in V1 and V2 of Macaque monkey revealed by optical imaging. Cereb. Cortex *Jun. 18.*

Mirabella, G., Bertini, G., Samengo, I., Kilavik, B. E., Frilli, D., Della Libera, C., and Chelazzi, L. (2007). Neurons in area V4 of the macaque translate attended visual features into behaviorally relevant categories. Neuron *54*, 303-318.

Motter, B. C. (2006). Modulation of transient and sustained response components of V4 neurons by temporal crowding in flashed stimulus sequences. J. Neurosci. *26*, 9683-9694.

Nelissen, K., Vanduffel, W., and Orban, G. A. (2006). Charting the lower superior temporal region, a new motion-sensitive region in monkey superior temporal sulcus. J. Neurosci. *26*, 5929-5947.

Pack, C. C., Berezovskii, V. K., and Born, R. T. (2001). Dynamic properties of neurons in cortical area MT in alert and anaesthetized macaque monkeys. Nature *414*, 905-908.

Pasupathy, A., and Connor, C. E. (1999). Responses to contour features in macaque area V4. J. Neurophysiol. *82*, 2490-2502.

Pollen, D. A., Przybyszewski, A. W., Rubin, M. A., and Foote, W. (2002). Spatial receptive field organization of macaque V4 neurons. Cereb. Cortex *12*, 601-616.

Reynolds, J. H., and Chelazzi, L. (2004). Attentional modulation of visual processing. Annu. Rev. Neurosci. *27*, 611-647.

Schein, S. J., and Desimone, R. (1990). Spectral properties of V4 neurons in the macaque. J. Neurosci. *10*, 3369-3389.

Schein, S. J., Marrocco, R. T., and de Monasterio, F. M. (1982). Is there a high concentration of color-selective cells in area V4 of monkey visual cortex? J. Neurophysiol. *47*, 193-213.

Schiller, P. H. (1993). The effects of V4 and middle temporal (MT) area lesions on visual performance in the rhesus monkey. Vis.l Neurosci. *10*, 717-746.

Schiller, P. H. (1996). On the specificity of neurons and visual areas. Behav. Brain. Res. *76*, 21-35.

Shipp, S., and Zeki, S. (1995). Segregation and convergence of specialised pathways in macaque monkey visual cortex. J. Anat. *187*, 547-562.

Smirnakis, S.M., Schmid, M.C., Weber, B., Tolias, A.S., Augath, M., Logothetis, N.K. (2007). Spatial specificity of BOLD versus cerebral blood volumn fMRI for mapping cortical organization. J. Cereb. Blood Flow Metab. *27*, 1248-61

Solomon, S. G., and Lennie, P. (2005). Chromatic gain controls in visual cortical neurons. J. Neurosci. *25*, 4779-4792.

Solomon, S. G., and Lennie, P. (2007). The machinery of colour vision. Nat. Rev. Neurosci. *8*, 276-286.

Stepniewska, I., Collins, C. E., and Kaas, J. H. (2005). Reappraisal of DL/V4 boundaries based on connectivity patterns of dorsolateral visual cortex in macaques. Cereb. Cortex *15*, 809-822.

Stockman, A., and Sharpe, L. T. (2000). The spectral sensitivities of the middle- and long-wavelength-sensitive cones derived from measurements in observers of known genotype. Vision Res. *40*, 1711-1737.

Tanaka, M., Weber, H., and Creutzfeldt, O. D. (1986). Visual properties and spatial distribution of neurones in the visual association area on the prelunate gyrus of the awake monkey. Exp. Brain Res. *65*, 11-37.

Tootell, R. B., Nelissen, K., Vanduffel, W., and Orban, G. A. (2004). Search for color 'center(s)' in macaque visual cortex. Cereb. Cortex *14*, 353-363.

Tsao, D. Y., Freiwald, W. A., Knutsen, T. A., Mandeville, J. B., and Tootell, R. B. (2003). Faces and objects in macaque cerebral cortex. Nat. Neurosci. *6*, 989-995.

Tsao, D. Y., Freiwald, W. A., Tootell, R. B., and Livingstone, M. S. (2006). A cortical region consisting entirely of face-selective cells. Science *311*, 670-674.

Van Essen, D. C., and Zeki, S. M. (1978). The topographic organization of rhesus monkey prestriate cortex. J. Physiol. *277*, 193-226.

Vanduffel, W., Fize, D., Mandeville, J. B., Nelissen, K., Van Hecke, P., Rosen, B. R., Tootell, R. B., and Orban, G. A. (2001). Visual motion processing investigated using contrast agent-enhanced fMRI in awake behaving monkeys. Neuron *32*, 565-577.

Wachtler, T., Sejnowski, T. J., and Albright, T. D. (2003). Representation of color stimuli in awake macaque primary visual cortex. Neuron *37*, 681-691.

Wade, A. R., Brewer, A. A., Rieger, J. W., and Wandell, B. A. (2002). Functional measurements of human ventral occipital cortex: retinotopy and colour. Philos. Trans. R. Soc. Lond. B Biol. Sci. *357*, 963-973.

Walsh, V., Carden, D., Butler, S. R., and Kulikowski, J. J. (1993). The effects of V4 lesions on the visual abilities of macaques: hue discrimination and colour constancy. Behavioural Brain Res. *53*, 51-62.

Xiao, Y., Zych, A., and Felleman, D. J. (1999). Segregation and convergence of functionally defined V2 thin stripe and interstripe compartment projections to area V4 of macaques. Cereb. Cortex *9*, 792-804.

Yoshioka, T., Levitt, J. B., and Lund, J. S. (1992). Intrinsic lattice connections of macaque monkey visual cortical area V4. J. Neurosci. *12*, 2785-2802.

Zeki, S. (1996). Are areas TEO and PIT of monkey visual cortex wholly distinct from the fourth visual complex (V4 complex)? Proc. R. Soc. Lond. B: Biol. Sci. *263*, 1539-1544.

Zeki, S., Watson, J. D., Lueck, C. J., Friston, K. J., Kennard, C., and Frackowiak, R. S. (1991). A direct demonstration of functional specialization in human visual cortex. J. Neurosci. *11*, 641-649.

Zeki, S. M. (1973). Colour coding in rhesus monkey prestriate cortex. Brain Res. *53*, 422-427.

Zeki, S. M. (1977). Colour coding in the superior temporal sulcus of rhesus monkey visual cortex. Proc. R. Soc. Lond. B: Biol. Sci. *197*, 195-223.

Zhao, F., Wang, P., Hendrich, K., Ugurbil, K., Kim, S.G. (2006) Cortical layer-dependent BOLD and CBV responses measured by spin-echo and gradient-echo fMRI: insights into hemodynamic regulation. Neuroimage *30*, 1139-60.

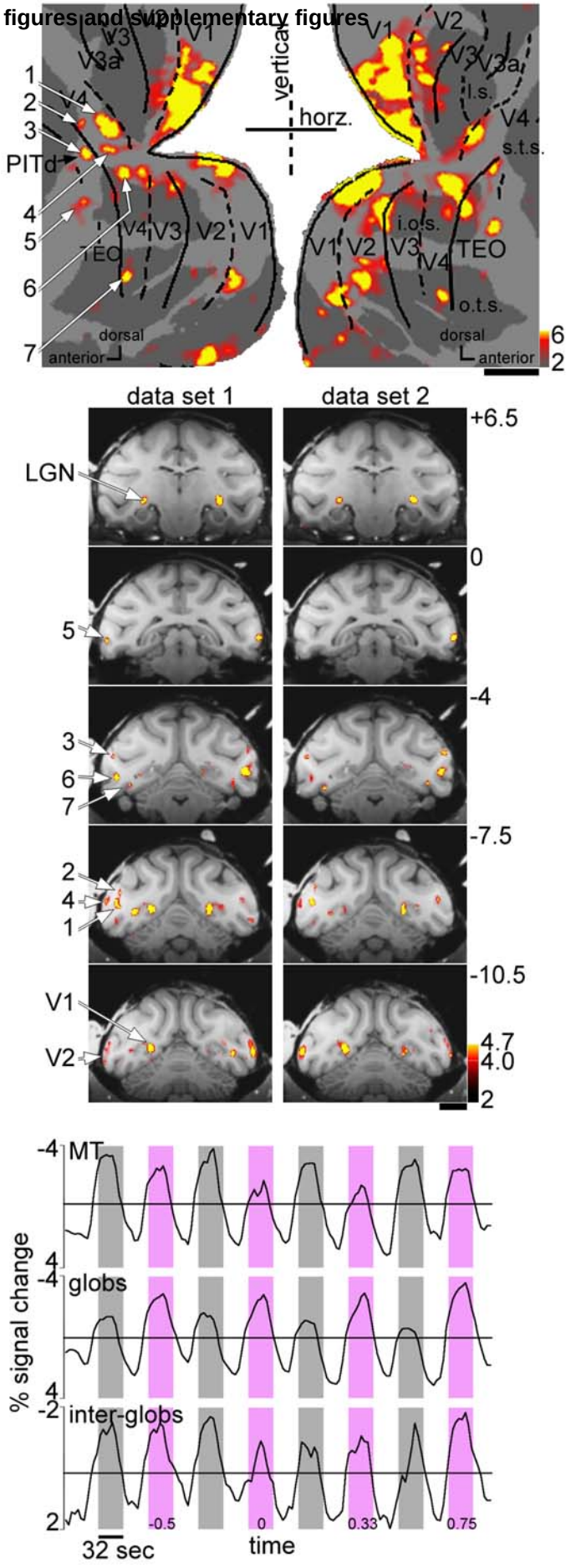

Figure 1, Conway et al., 2007

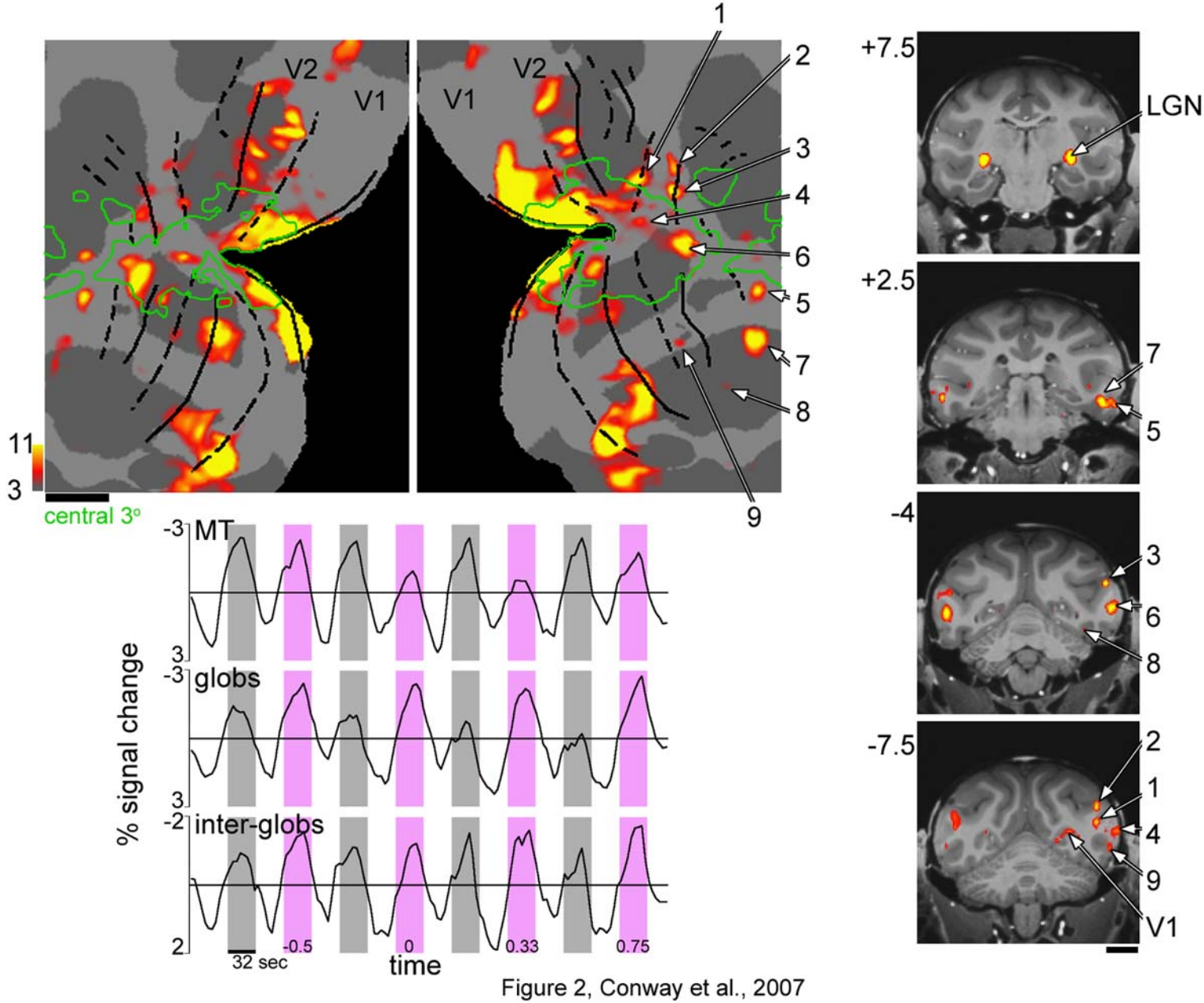

Figure 2, Conway et al., 2007

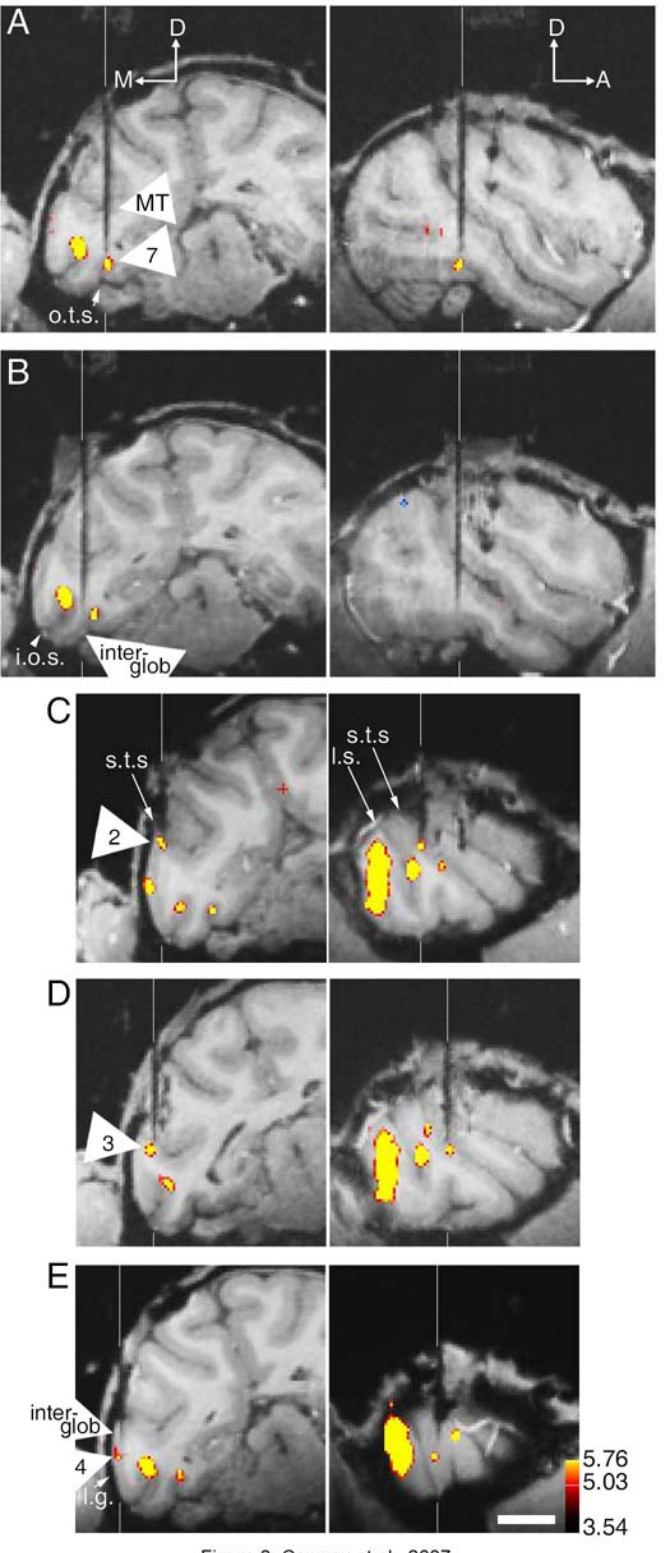

Figure 3, Conway et al., 2007

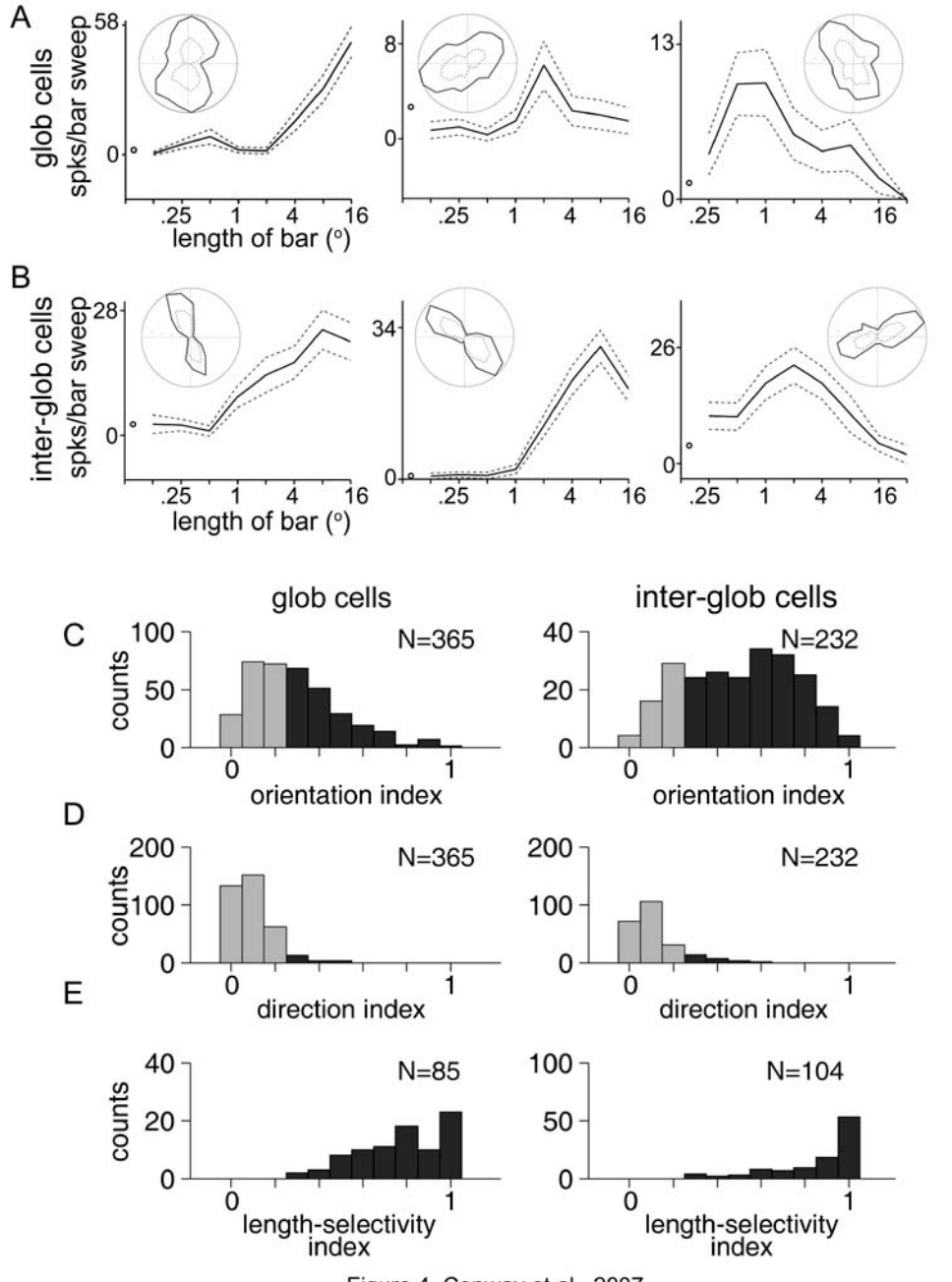

Figure 4, Conway et al., 2007

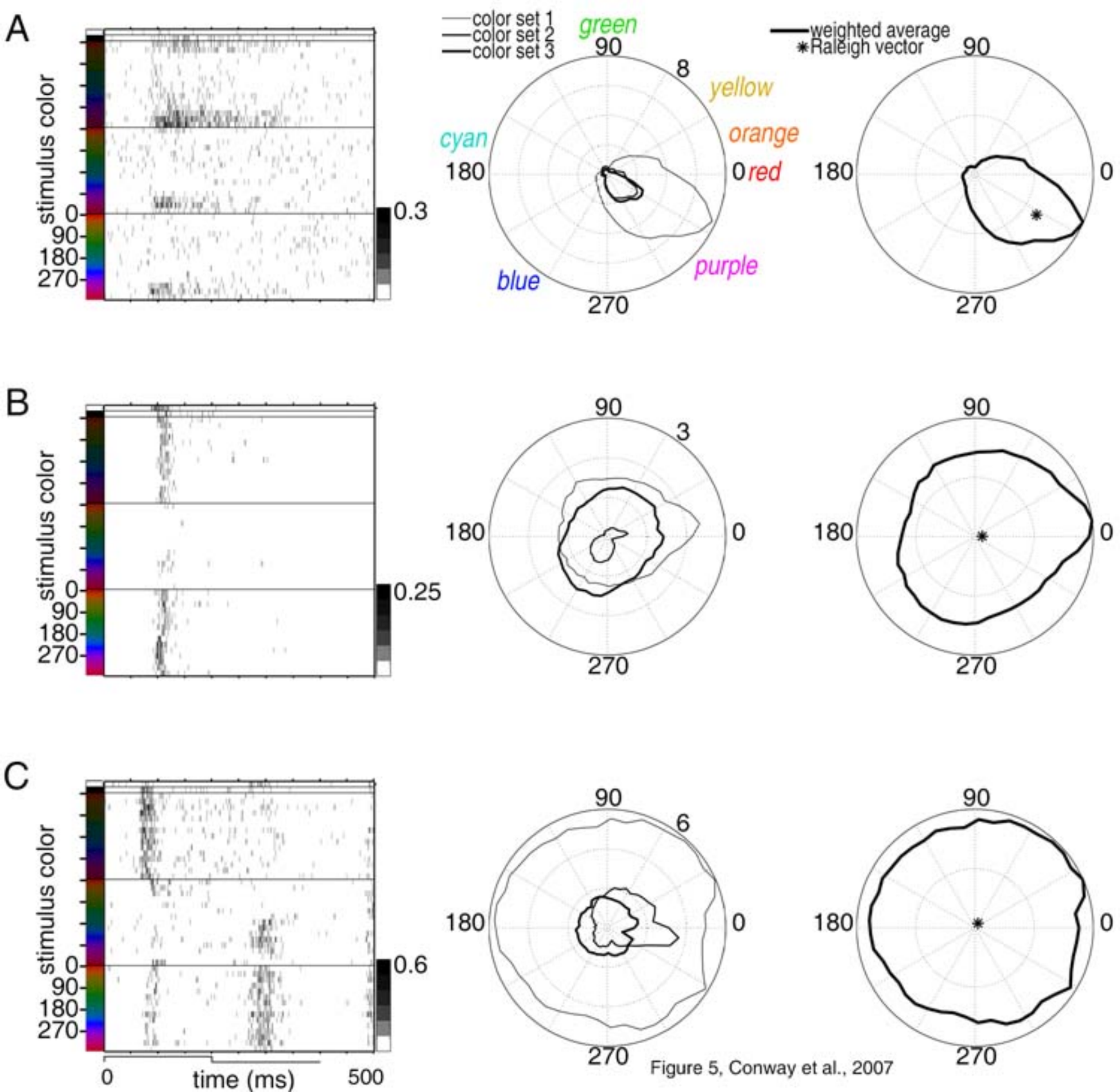

Figure 5, Conway et al., 2007

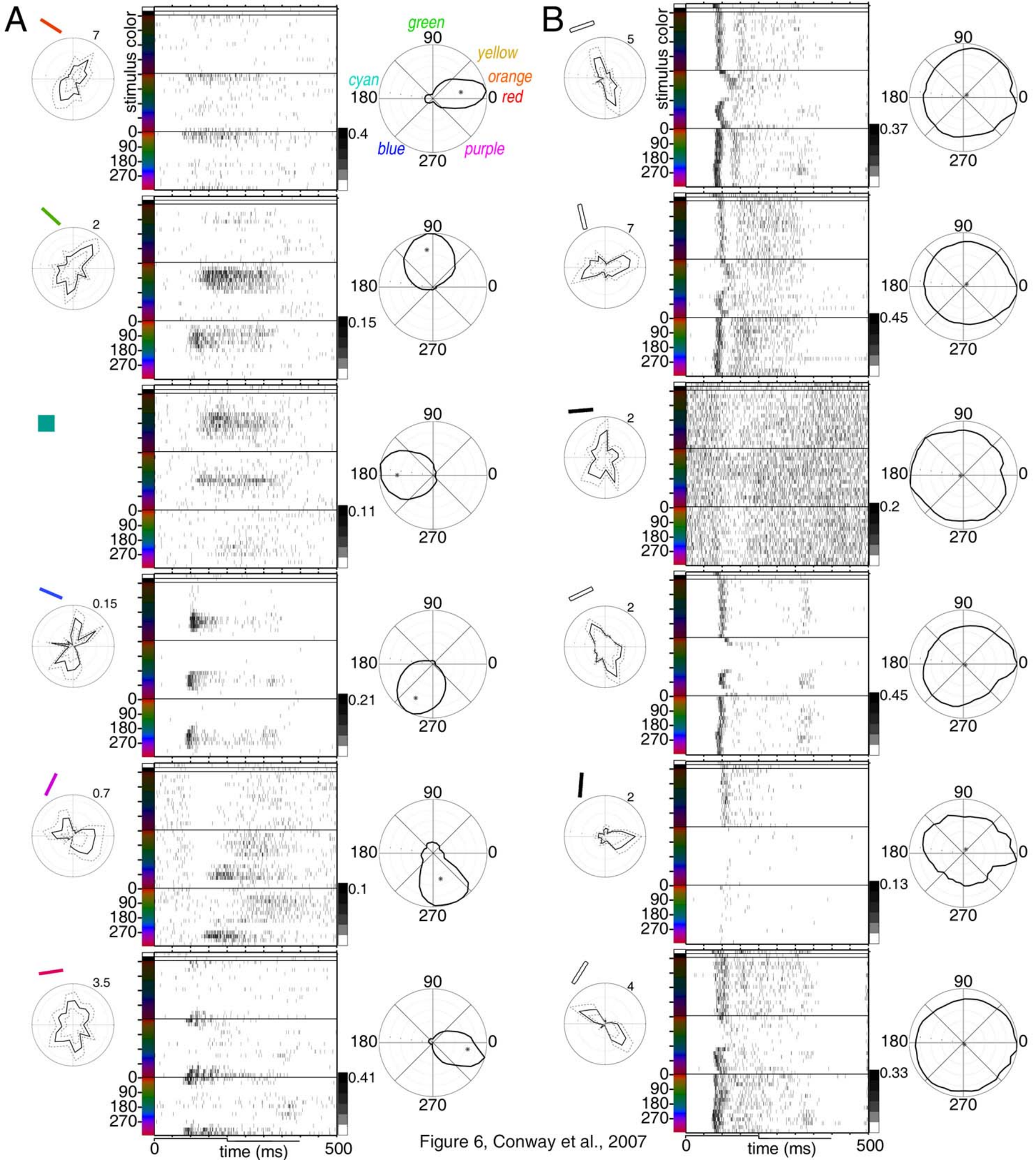

Figure 6, Conway et al., 2007

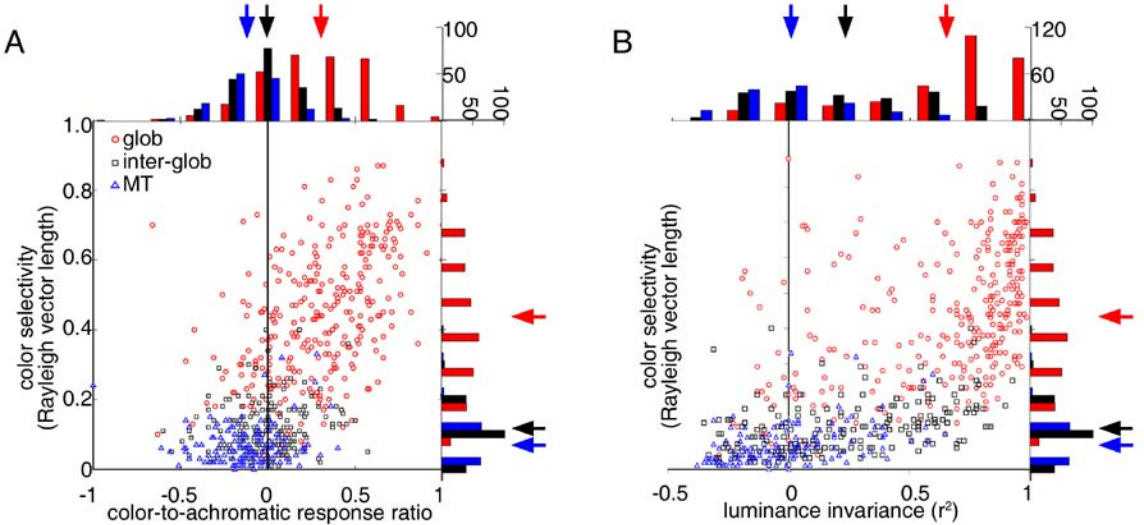

Figure 7, Conway et al., 2007

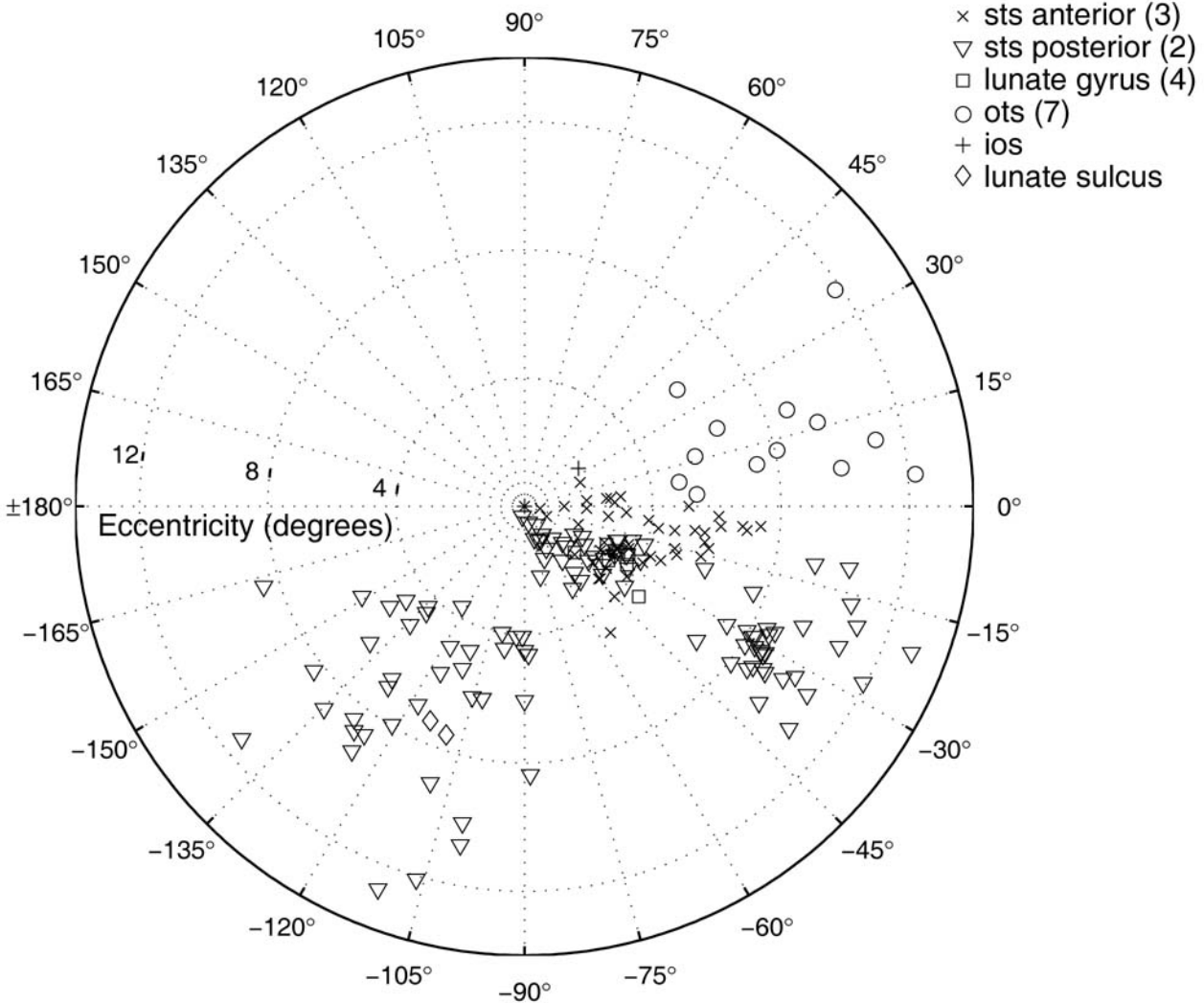

Figure 8, Conway et al., 2007

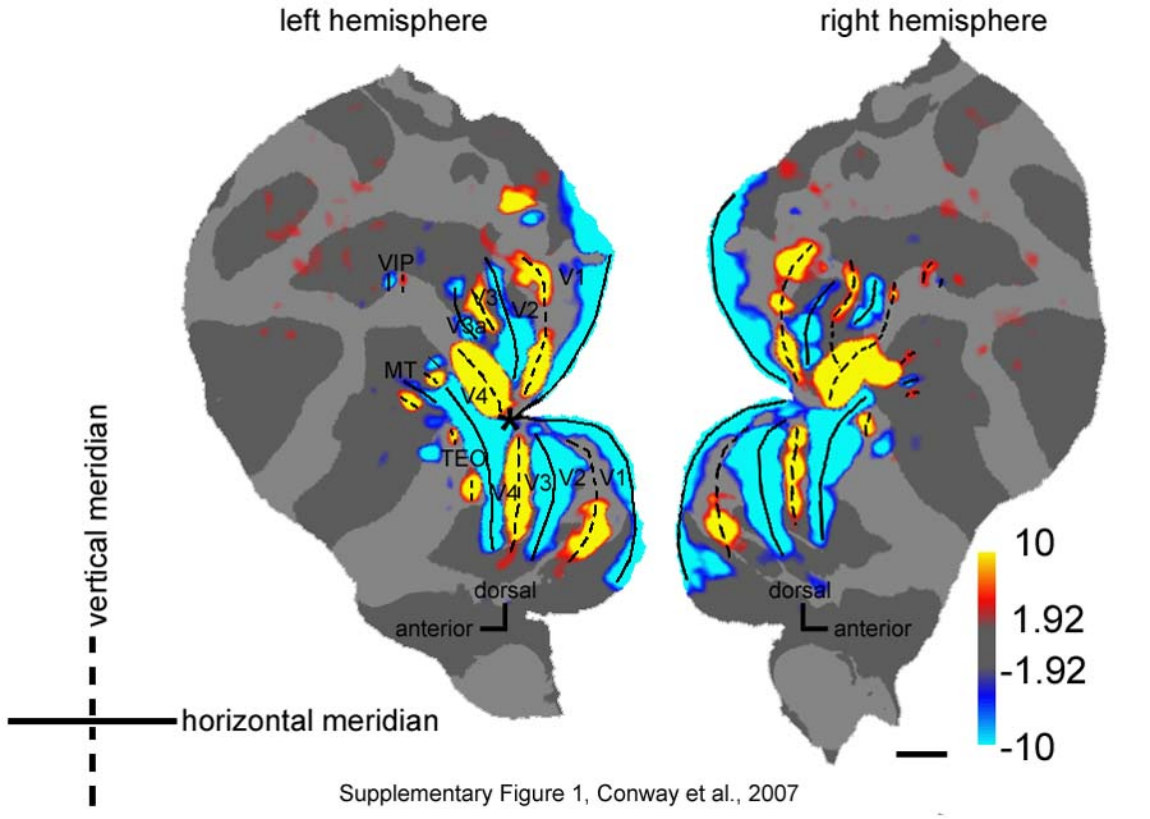

Supplementary Figure 1, Conway et al., 2007

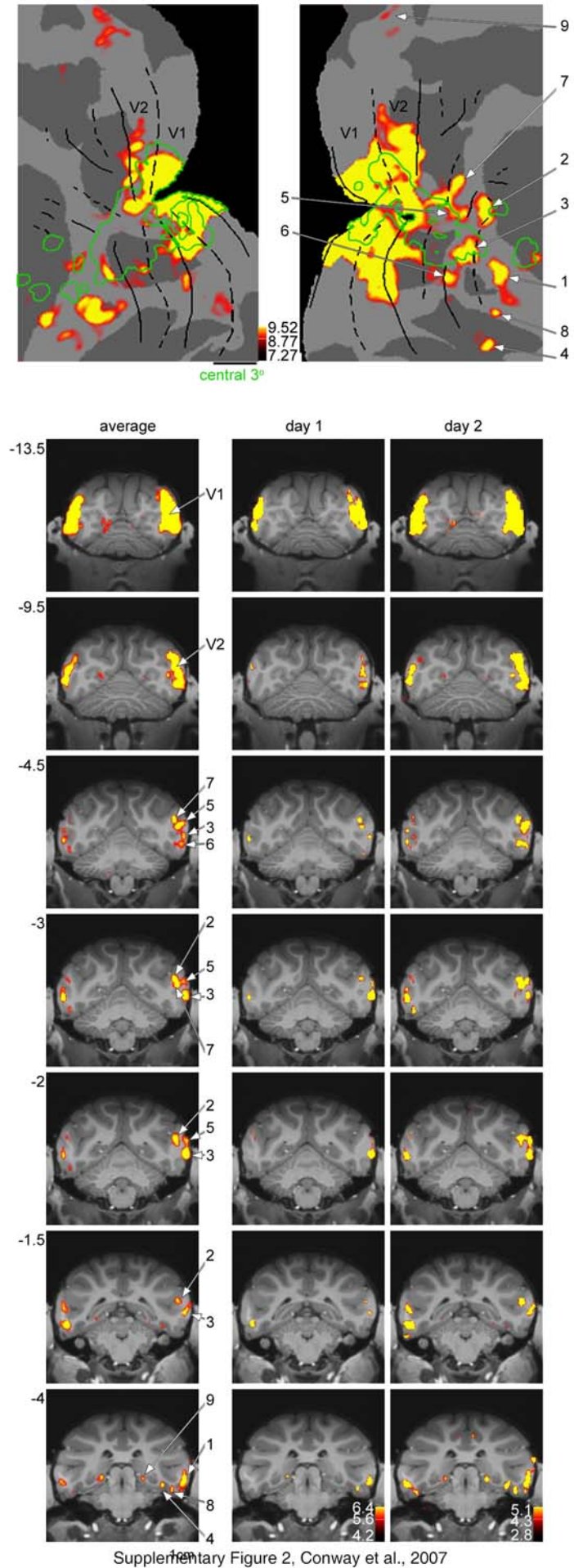

Supplementary Figure 2, Conway et al., 2007

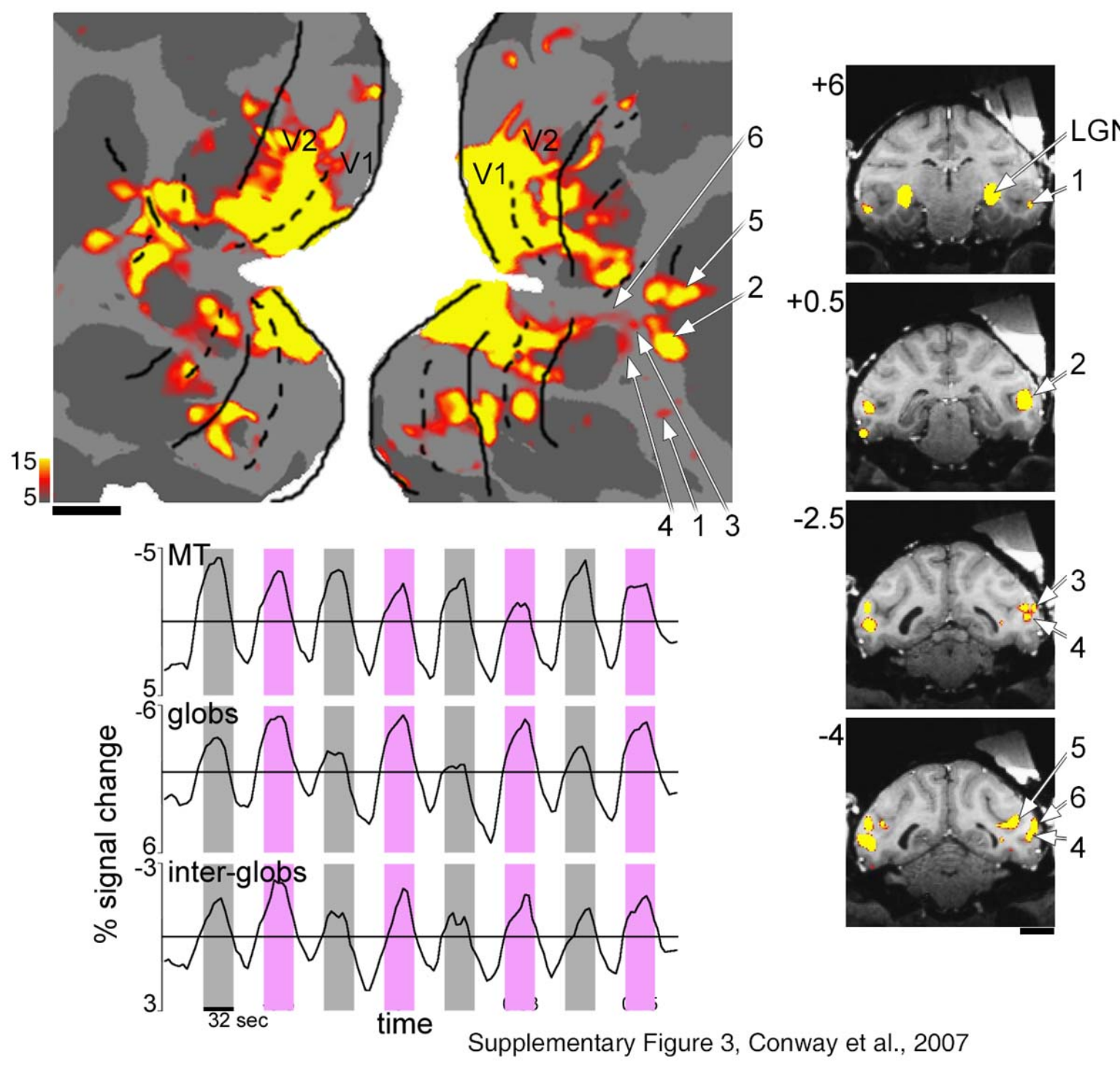

Supplementary Figure 3, Conway et al., 2007

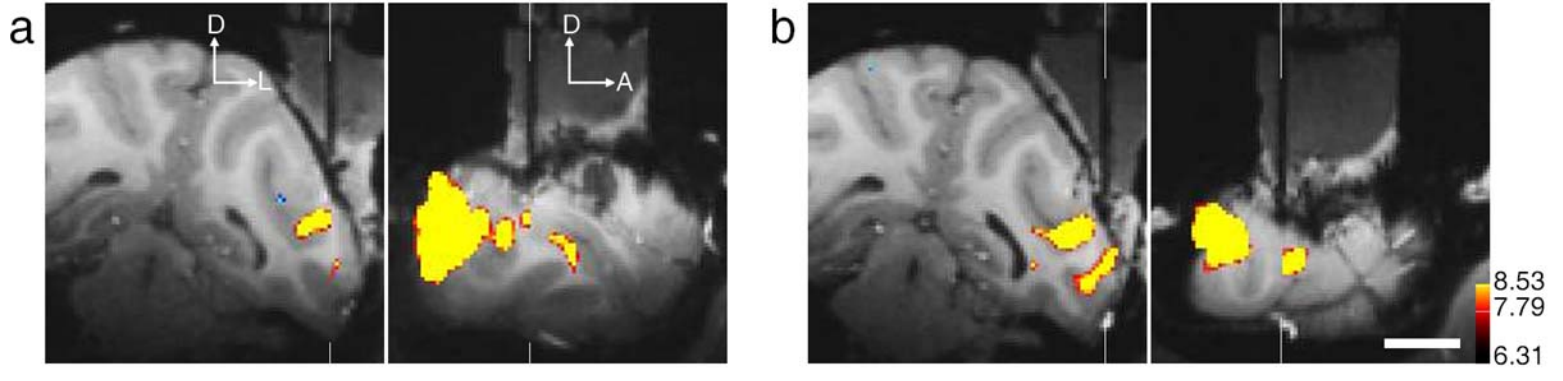

Supplementary Figure 4, Conway et al., 2007

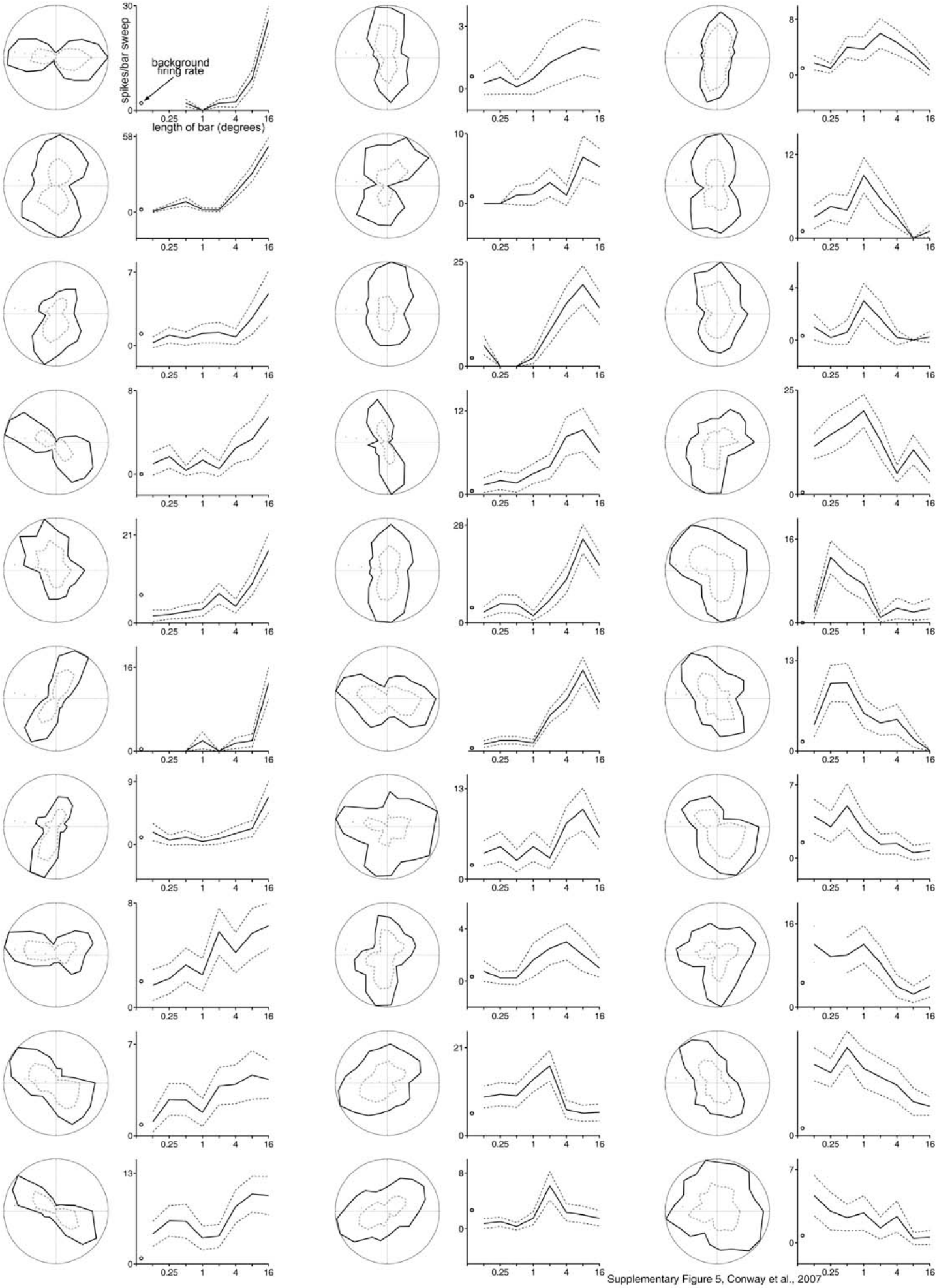

Supplementary Figure 5, Conway et al., 2007

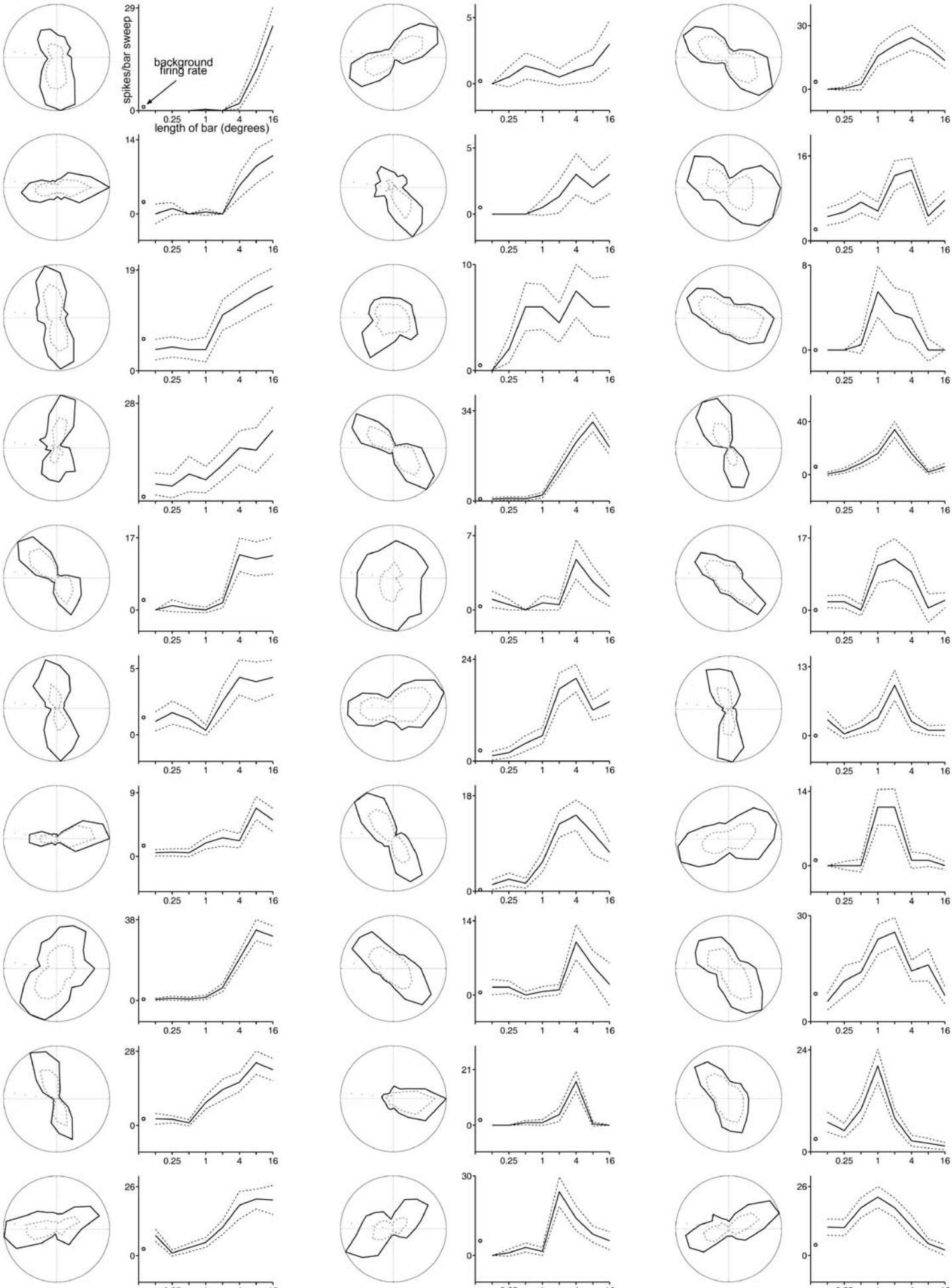

Supplementary Figure 6, Conway et al., 2007

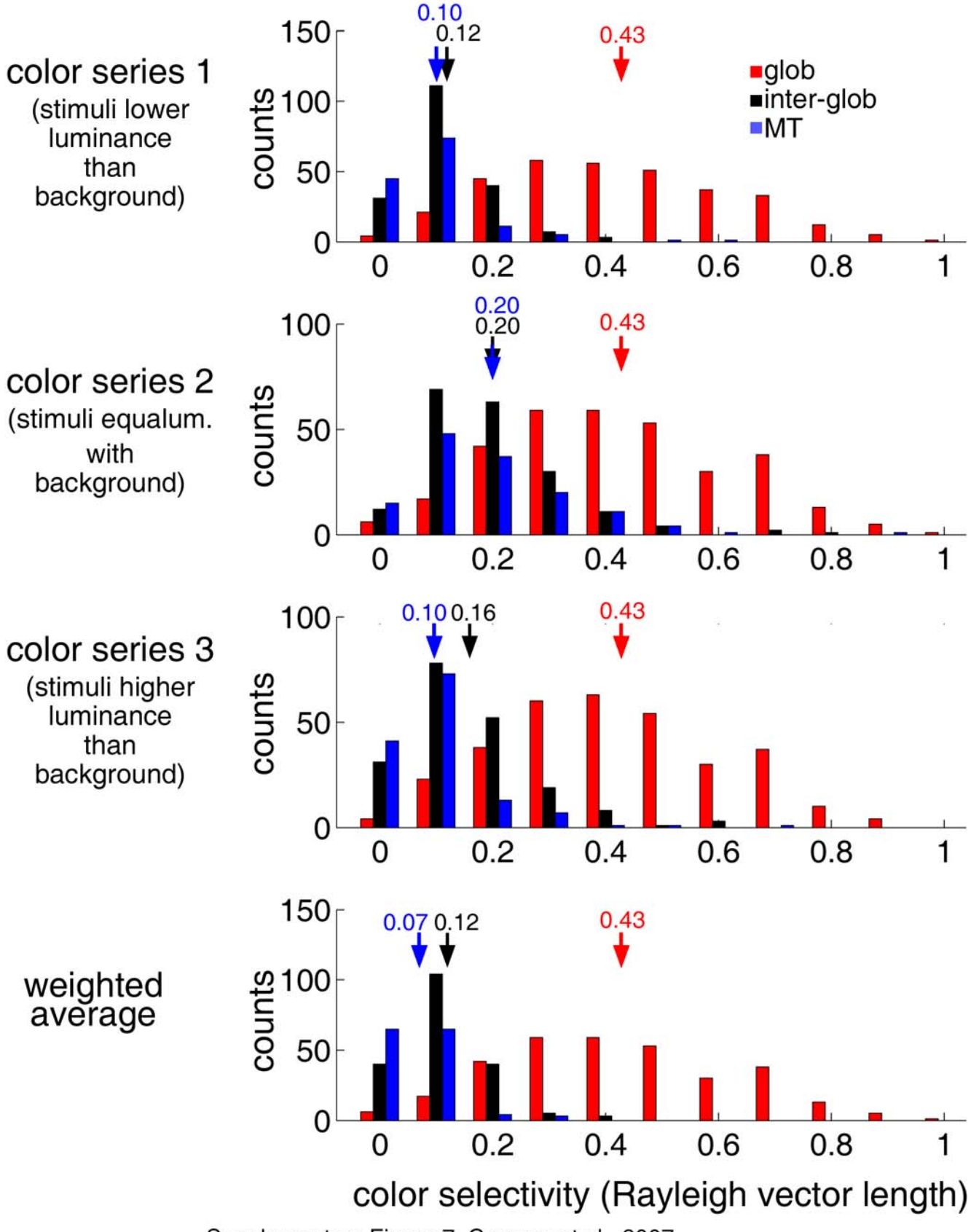

Supplementary Figure 7, Conway et al., 2007

Supplementary Figure 8, Conway et al., 2007

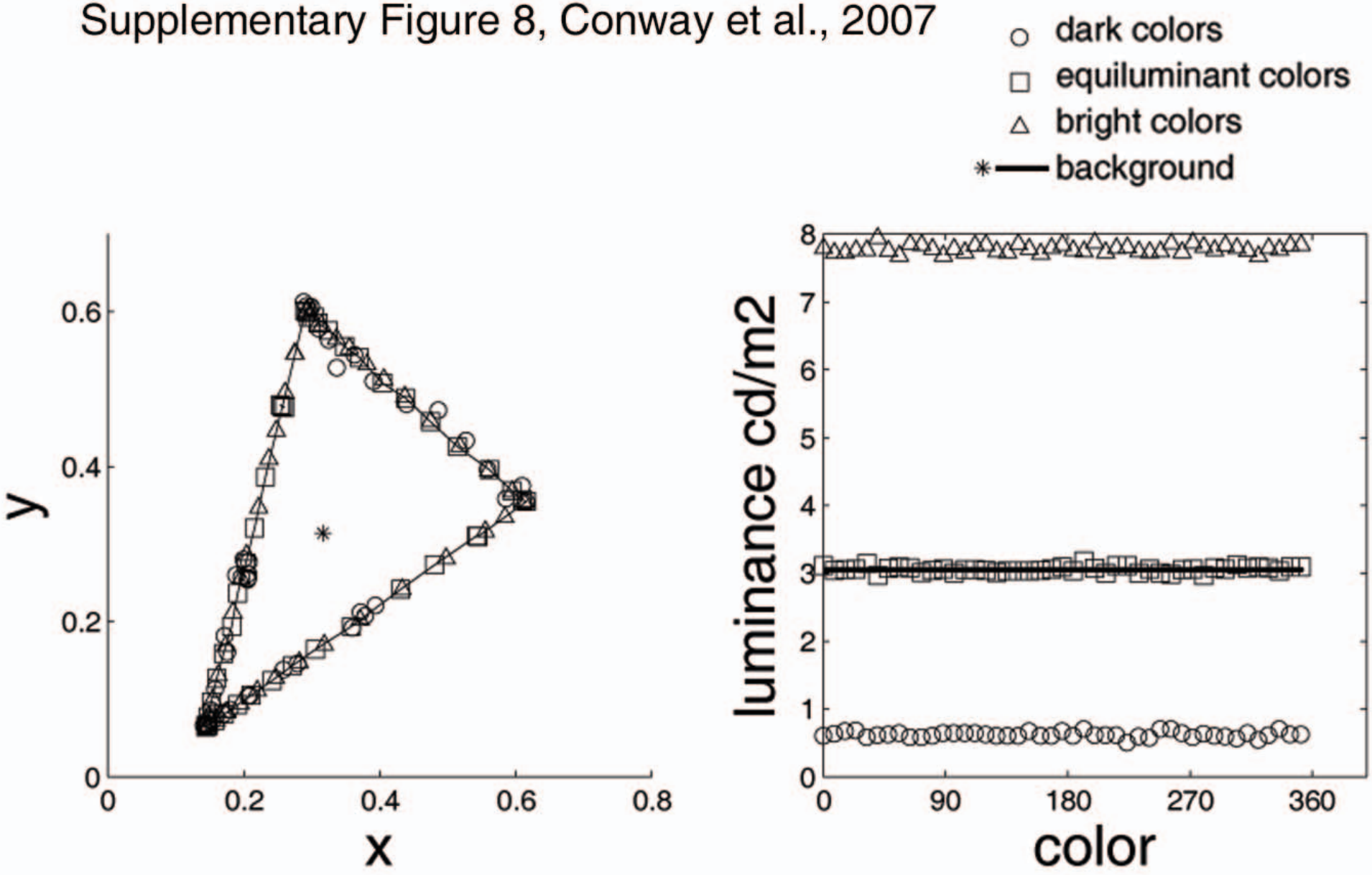

	Dark colors			Equiluminant colors			Bright colors		
color	**x**	**y**	**Luminance (cd/m2)**	**x**	**y**	**Luminance (cd/m2)**	**x**	**y**	**Luminance (cd/m2)**
0	0.616	0.354	0.6	0.616	0.355	3.11	0.615	0.354	7.8
8	0.61	0.375	0.63	0.61	0.357	3.04	0.611	0.355	7.73
16	0.586	0.359	0.67	0.594	0.369	3.05	0.595	0.368	7.73
24	0.559	0.396	0.68	0.561	0.396	3.06	0.56	0.395	7.77
32	0.528	0.434	0.58	0.515	0.426	3.14	0.518	0.427	7.77
40	0.487	0.473	0.61	0.475	0.458	2.96	0.475	0.459	7.95
48	0.44	0.481	0.62	0.438	0.489	3.07	0.437	0.49	7.76
56	0.391	0.51	0.64	0.404	0.508	3.09	0.406	0.513	7.69
64	0.337	0.528	0.58	0.37	0.541	3.08	0.381	0.532	7.86
72	0.363	0.544	0.58	0.348	0.555	3.01	0.355	0.553	7.85
80	0.292	0.607	0.6	0.324	0.576	3.04	0.336	0.565	7.79
88	0.299	0.606	0.64	0.309	0.585	3.06	0.314	0.583	7.69
96	0.31	0.578	0.64	0.303	0.593	3	0.298	0.596	7.79
104	0.325	0.564	0.64	0.292	0.599	3.05	0.297	0.597	7.74
112	0.299	0.605	0.64	0.295	0.593	3.05	0.293	0.601	7.84
120	0.288	0.612	0.62	0.29	0.601	3.04	0.291	0.599	7.85
128	0.189	0.26	0.6	0.257	0.477	3.01	0.274	0.546	7.75
136	0.206	0.254	0.6	0.26	0.476	3.03	0.275	0.546	7.74
144	0.206	0.255	0.6	0.254	0.48	3.03	0.261	0.496	7.86
152	0.2	0.28	0.67	0.257	0.478	3.03	0.248	0.447	7.79
160	0.207	0.262	0.6	0.232	0.387	3.04	0.237	0.41	7.72
168	0.197	0.258	0.6	0.216	0.321	3.06	0.222	0.347	7.8
176	0.208	0.278	0.67	0.203	0.276	3.09	0.204	0.286	7.85
184	0.207	0.257	0.6	0.191	0.237	3.03	0.196	0.256	7.77
192	0.172	0.182	0.7	0.182	0.194	3.18	0.184	0.212	7.75
200	0.176	0.161	0.61	0.17	0.159	3.07	0.173	0.169	7.88
208	0.158	0.113	0.61	0.16	0.127	3	0.162	0.131	7.74
216	0.152	0.086	0.61	0.152	0.096	3.11	0.154	0.1	7.8
224	0.148	0.074	0.5	0.147	0.077	3.11	0.148	0.078	7.81
232	0.145	0.068	0.59	0.144	0.067	3	0.145	0.066	7.75
240	0.141	0.066	0.57	0.144	0.064	3.06	0.144	0.064	7.74
248	0.145	0.066	0.7	0.144	0.064	3	0.145	0.064	7.75
256	0.147	0.066	0.7	0.147	0.066	2.98	0.149	0.067	7.87
264	0.154	0.072	0.64	0.157	0.072	3.05	0.159	0.073	7.74
272	0.17	0.081	0.58	0.171	0.081	3.06	0.175	0.083	7.88
280	0.18	0.087	0.63	0.191	0.093	2.96	0.195	0.095	7.82
288	0.21	0.105	0.6	0.211	0.105	3.08	0.22	0.111	7.77
296	0.207	0.104	0.59	0.242	0.124	3.06	0.247	0.128	7.84
304	0.259	0.138	0.56	0.271	0.143	3.12	0.281	0.148	7.8
312	0.279	0.146	0.64	0.305	0.164	3.08	0.318	0.17	7.76
320	0.36	0.192	0.54	0.358	0.194	3.09	0.371	0.203	7.68
328	0.372	0.212	0.61	0.431	0.242	3.08	0.433	0.242	7.8
336	0.394	0.221	0.7	0.481	0.273	3.03	0.498	0.282	7.78
344	0.379	0.208	0.62	0.542	0.311	3.09	0.555	0.317	7.84
352	0.379	0.208	0.62	0.544	0.31	3.09	0.584	0.335	7.85

Background: (x,y, luminance): 0.316, 0.314, 3.05 cd/m2; **white**: 0.274, 0.303, 77.4 cd/m2； **black**:0.02 cd/m2

Supplementary Table 1

	Dark colors			Equiluminant colors			Bright colors		
color	**x**	**y**	**Luminance (cd/m2)**	**x**	**y**	**Luminance (cd/m2)**	**x**	**y**	**Luminance (cd/m2)**
0	0.616	0.354	0.6	0.616	0.355	3.11	0.615	0.354	7.8
8	0.61	0.375	0.63	0.61	0.357	3.04	0.611	0.355	7.73
16	0.586	0.359	0.67	0.594	0.369	3.05	0.595	0.368	7.73
24	0.559	0.396	0.68	0.561	0.396	3.06	0.56	0.395	7.77
32	0.528	0.434	0.58	0.515	0.426	3.14	0.518	0.427	7.77
40	0.487	0.473	0.61	0.475	0.458	2.96	0.475	0.459	7.95
48	0.44	0.481	0.62	0.438	0.489	3.07	0.437	0.49	7.76
56	0.391	0.51	0.64	0.404	0.508	3.09	0.406	0.513	7.69
64	0.337	0.528	0.58	0.37	0.541	3.08	0.381	0.532	7.86
72	0.363	0.544	0.58	0.348	0.555	3.01	0.355	0.553	7.85
80	0.292	0.607	0.6	0.324	0.576	3.04	0.336	0.565	7.79
88	0.299	0.606	0.64	0.309	0.585	3.06	0.314	0.583	7.69
96	0.31	0.578	0.64	0.303	0.593	3	0.298	0.596	7.79
104	0.325	0.564	0.64	0.292	0.599	3.05	0.297	0.597	7.74
112	0.299	0.605	0.64	0.295	0.593	3.05	0.293	0.601	7.84
120	0.288	0.612	0.62	0.29	0.601	3.04	0.291	0.599	7.85
128	0.189	0.26	0.6	0.257	0.477	3.01	0.274	0.546	7.75
136	0.206	0.254	0.6	0.26	0.476	3.03	0.275	0.546	7.74
144	0.206	0.255	0.6	0.254	0.48	3.03	0.261	0.496	7.86
152	0.2	0.28	0.67	0.257	0.478	3.03	0.248	0.447	7.79
160	0.207	0.262	0.6	0.232	0.387	3.04	0.237	0.41	7.72
168	0.197	0.258	0.6	0.216	0.321	3.06	0.222	0.347	7.8
176	0.208	0.278	0.67	0.203	0.276	3.09	0.204	0.286	7.85
184	0.207	0.257	0.6	0.191	0.237	3.03	0.196	0.256	7.77
192	0.172	0.182	0.7	0.182	0.194	3.18	0.184	0.212	7.75
200	0.176	0.161	0.61	0.17	0.159	3.07	0.173	0.169	7.88
208	0.158	0.113	0.61	0.16	0.127	3	0.162	0.131	7.74
216	0.152	0.086	0.61	0.152	0.096	3.11	0.154	0.1	7.8
224	0.148	0.074	0.5	0.147	0.077	3.11	0.148	0.078	7.81
232	0.145	0.068	0.59	0.144	0.067	3	0.145	0.066	7.75
240	0.141	0.066	0.57	0.144	0.064	3.06	0.144	0.064	7.74
248	0.145	0.066	0.7	0.144	0.064	3	0.145	0.064	7.75
256	0.147	0.066	0.7	0.147	0.066	2.98	0.149	0.067	7.87
264	0.154	0.072	0.64	0.157	0.072	3.05	0.159	0.073	7.74
272	0.17	0.081	0.58	0.171	0.081	3.06	0.175	0.083	7.88
280	0.18	0.087	0.63	0.191	0.093	2.96	0.195	0.095	7.82
288	0.21	0.105	0.6	0.211	0.105	3.08	0.22	0.111	7.77
296	0.207	0.104	0.59	0.242	0.124	3.06	0.247	0.128	7.84
304	0.259	0.138	0.56	0.271	0.143	3.12	0.281	0.148	7.8
312	0.279	0.146	0.64	0.305	0.164	3.08	0.318	0.17	7.76
320	0.36	0.192	0.54	0.358	0.194	3.09	0.371	0.203	7.68
328	0.372	0.212	0.61	0.431	0.242	3.08	0.433	0.242	7.8
336	0.394	0.221	0.7	0.481	0.273	3.03	0.498	0.282	7.78
344	0.379	0.208	0.62	0.542	0.311	3.09	0.555	0.317	7.84
352	0.379	0.208	0.62	0.544	0.31	3.09	0.584	0.335	7.85

Background: (x,y, luminance): 0.316, 0.314, 3.05 cd/m2; **white**: 0.274, 0.303, 77.4 cd/m2； **black**:0.02 cd/m2